Recent Changes to Langjökull Icecap, Iceland:
An investigation integrating airborne LiDAR and satellite imagery

Allen J. Pope

12 June 2009

A dissertation presented in partial fulfillment of the requirements
for the degree of Master of Philosophy in Polar Studies

Scott Polar Research Institute
University of Cambridge
Lensfield Road
Cambridge CB2 1ER

Trinity College
University of Cambridge
Trinity Street
Cambridge CB2 1TQ

Abstract

Langjökull, Iceland's second largest icecap (~950 km^2), was the subject of an incomplete airborne LiDAR survey in August 2007. This study investigates and evaluates the application of photoclinometry, which employs visible light imagery (here, Landsat ETM+ band 4) to interpolate unmeasured sections of this fragmented data set. A complete digital elevation model (DEM) of Langjökull was produced, and photoclinometry was determined to be a satisfactory and robust technique for topographic interpolation (RMS error = 3.4 m over a 3 km section). Future applications of photoclinometry can ensure optimal results by focusing on the consistent ability of their imager to accurately represent low contrast surfaces; also, consideration of setting characteristic such as solar azimuth, solar elevation, and moderate surface slope will make photoclinometric interpolation more effective. Photoclinometry it is proven to be a current and valuable technique, it is confirmed as a secondary rather than primary tool, and other possible applications of photoclinometry are considered.

Using the completed DEM of Langjökull for summer 2007 and a previously prepared corresponding 1997 data set, Langjökull was found to have a specific annual mass balance of -0.99 ± 0.1 meters per year of water equivalence (m yr^{-1} w.e.), a number which confirms published predictions that Langjökull will likely disappear in the next 200 years. Comparison of remotely-sensed mass balance values and traditional *in situ* measurements revealed a possible systematic disparity; it is hypothesized that field measurements may not be sufficiently constraining behavior of interior areas and that the signal from strongly receding outlet glaciers may be skewing the *in situ* mass balance value calculated for the entire icecap. An additional DEM of outlet Hagafellsjökull Vestari allowed for calculation of specific mass balances of -2.28 m yr^{-1} w.e. for 1997-2001, -3.86 m yr^{-1} w.e. for 2001-2007, and -3.23 m yr^{-1} w.e. for 1997-2007. Similarly, visual inspection and tracing of Landsat images showed a recession of -3.4 ± 2.5 km^2 yr^{-1} from 1994 to 2007. The new 2007 DEM allowed for clear visualization of strong recession on several Langjökull outlets as well as interior mass loss and terminus advance witnessing to the 1998 surge event of outlet Hagafellsjökull Eystri. In addition, slight interior elevation increase and anti-correlated mass loss and terminal retreat potentially indicate a future surge of outlet Hagafellsjökull Vestari.

In sum, the technological and glaciological information put forward in this study provides a method for innovative cryospheric research, presents a much needed benchmark and update on the state of Langjökull, and ultimately facilitates and encourages continued monitoring of highly important smaller glaciers and icecaps.

Table of Contents

List of Figures

List of Tables

Acknowledgements

A dissertation is a daunting process for any MPhil student approaching it, and I would like to sincerely thank all the people that made this an incredibly beneficial and enjoyable experience.

First and foremost I am deeply indebted to my advisor, Dr. Gareth Rees, for giving me the opportunity to work on this project, guiding me, putting up with my questions and emails, and nurturing my interest in polar remote sensing. I look forward to our future work together and know that there is a lot to learn from him.

Many thanks to Drs. Ian Willis, Neil Arnold, and Poul Christoffersen for feedback, suggestions, encouragement, and discussions along the way.

I am deeply indebted to Helgi Björnsson and Finnur Pálsson at the University of Iceland's Earth Science Institute for providing extensive data concerning Langjökull. Similarly, Richard Hodgkins at Loughborough University and Adrian Fox at the British Antarctic Survey provided a very useful 2001 DEM of the terminus of Hagafellsjökull Vestari.

I must also express my gratitude to Trinity College, Cambridge for supporting me throughout my course. This course of study would not have been an option for me otherwise.

And finally, thanks to family, friends, and fellow students at SPRI and Trinity College for help settling into life in Cambridge, the opportunity to enjoy and make the most out of this MPhil, and companionship throughout the entire working process.

Declaration

I declare that this thesis is my own unaided work, except where noted above and in the text. It is no more than 20,000 words in length, excluding acknowledgements, declaration, references, tables, lists, and captions.

1. Introduction

While emphasis has been placed on a comprehensive understanding of the continental ice sheets because of their potential to raise global sea level by over 70 m (Anderson 1999), in the present day 60% of ice-melt contribution to sea level rise is traced to significantly smaller ice caps and glaciers which respond much more quickly to shifting climate (Meier et al. 2007; IPCC 2007). Of particular relevance to this study, a not-insignificant contribution comes from the icecaps and glaciers of Iceland (Oerlemans et al. 2005). 11% of Iceland is glaciated, with enough ice locked away in glaciers and icecaps to produce 3600 km^3 of liquid water or raise sea level by 1 cm. Storing an equivalent of 20 years of the country's precipitation, Iceland's glaciers provide over 30% of river water which is subsequently harnessed not only for agriculture and human consumption but essential hydropower resources (Björnsson & Pálsson 2008). Iceland's changing glacial state is thus significant on both global and local scales.

Annual glacier mass balance[1] is a very sensitive indicator of response to a changing environment (Pelto & Riedel 2001) whether due to changing precipitation, temperature, or some other forcing factor. Admittedly, glacier mass balance can be convoluted by glacier orientation and local and regional geographical concerns, but by combining glacier observations into a regional network, these factors can be identified and quantified (Holmlund & Jansson 1999; Pelto & Riedel 2001). By distinguishing between net mass balance and other glacier responses, such as changes in elevation distribution or terminal retreat, a more nuanced picture of glacier response to climate can be built (Miller & Pelto 1990; 1999). Alpine glacier mass balance records stretch back to 1946 in North America (Miller & Pelto 1990) and 1945 in Europe (Holmlund & Jansson 1999); these records not only show a response to climatic warming early in the 20th century (Holmlund & Jansson 1999), but also a modern response to currently warming temperatures in certain areas (Miller & Pelto 1999).

The changing state of these smaller ice caps and glaciers has significant implications for sea level rise, water resource availability, and geomorphologic hazards for populations all over the world (Richardson & Reynolds 2000). However, due to wide spatial distribution and typically harsh and rugged conditions, extensive studies of smaller glaciers are lacking. In addition to studying net mass balance and margin tracking, quantifying the spatial distribution of mass loss facilitates a better understanding of the dynamic physical response of the glaciers in question (e.g. Hagen et al. 2005). It is essential to study the behavior of mountain glaciers

[1] Glacier mass balance – the difference between annual accumulation (snowfall) and ablation (melt, runoff, and sublimation) measured in meters of water equivalent (m.w.e.)

and icecaps in order to fully understand the changes that they are currently experiencing and therefore the continued global effects they will have (e.g. Haeberli et al. 1999).

1.1 Icelandic Glaciers

As mentioned above, small Arctic glaciers play a significant role in Earth's current climate system. While many Arctic glaciers sustain low seasonal mass balances and small interannual variability, Icelandic glaciers attribute their exceptionally large seasonal mass balance and interannual variability to a largely maritime climate regime (Braithwaite 2005). While some studies have used present day Icelandic glaciers as analogues for past ice sheet behavior (e.g. Evans et al. 1999), many Icelandic glaciers are considered unique because of the widespread interaction of glacial and volcanic systems (Björnsson et al. 2001) which can cause not only unpredictable flow dynamics but destructive jökulhlaup[2] events (Björnsson 2002).

Iceland's glaciated areas are dominated by highland icecaps which have smaller outlet glaciers (see Figure 1.1). Every one of these major icecaps is characterized by at least one surge-type outlet glacier (Björnsson et al. 2003). Succinctly, surge events are part of a cycle of

Figure 1.1 *Sketch map showing Iceland's major icecaps (Williams et al. 1997). Langjökull is in west-central Iceland.*

[2] Jökulhlaup – a glacier outburst flood, often caused by subglacial volcanic activity

mass accumulation and expulsion. While steeply-sloping glaciers are able to maintain a steady state balance between accumulation and ablation, surge-type glaciers are generally characterized by a gentle surface slope which results in a velocity too low to sustain a flux commensurate with their accumulation rate (Björnsson et al. 2003). Therefore, after a slight increase in flow for 2-3 years and the development and progression of a surface bulge, episodic events when the glacier dramatically increases flow rate (by orders of magnitude) contribute significantly to the glacier's total mass transfer (Björnsson & Pálsson 2008). While Icelandic surge events are neither regular nor correlated to glacier size or mass balance (Björnsson et al. 2003), historical reports of glacier surges go back centuries, with Vatnajökull's outlet Brúarjökull having the longest history of surging (as far back as 1625; Hall et al. 1995b). In addition to pushing forward the glacier terminus by kilometers, surge events significantly increase the sediment load in proglacial rivers (Björnsson et al. 2003) as well as displacing glacier water divides and decreasing the surface area of upper-icecap accumulation zones (Magnússon et al. 2004).

On a wider scale than surge events, Iceland's placement in the North Atlantic convergence zone of warm and cold air and water masses makes it an ideal location to study climate signals which can be uniquely registered in its glaciers (Brown et al. 1999; McKinzey et al. 2005a). Although response time depends on the size of the glacier or ice cap in question (Kirkbride & Dugmore 2006), typically a response to a climate shift is seen at the glacier snout of an Icelandic icecap within a decade (Sigurðsson & Jónsson 1995). In addition to global climate shifts, Icelandic climate can be partly described by patterns governed by the North Atlantic Oscillation (NAO; see Figure 1.2). The NAO goes through strong and weak cycles, creating a dipole across the Atlantic between 30 and 70 degrees north, at times giving continental Europe dry, warm winters and Iceland and Greenland cool conditions with increased precipitation and vice versa (Hurrell 1995; Bradwell et al. 2006). While glacier behavior in Svalbard does not correlate with NAO activity (Rasmussen & Kohler 2007), Bradwell et al. (2006) document that the speed and timing of advance of southern Icelandic glaciers indicates response to NAO activity. Interestingly, although surge events are not

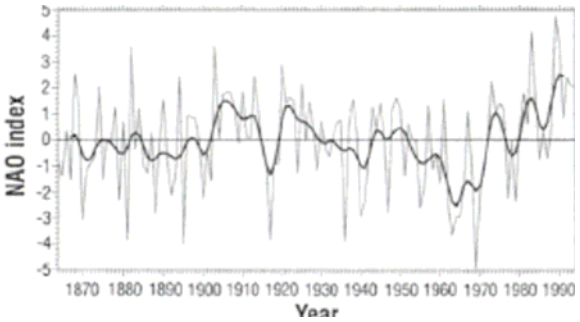

Figure 1.2 *Winter (December-March) index of the NAO based on the difference of normalized pressures between Lisbon, Portugal, and Stykkisholmur, Iceland, from 1864 to 1994. The heavy solid line is smoothed with a low pass filter to remove fluctuations with periods less than 4 years (Hurrell 1995).*

correlated with climatic changes, the maximum extension at the end of surges and the minimum extent before surging do appear to be influenced by long term climate shifts (Sigurðsson & Jónsson 1995). Since 1930, all Icelandic glaciers, especially non-surge type, show a clear response to climatic variation; this shift has been related to temperature rather than any change in precipitation as there has been no noticeable shift in the latter over the 20th century (Jóhannesson & Sigurðsson 1998). Indeed, Icelandic glacier response to the NAO is largely a superposition over broader climatic changes; although the cooling of the 1940s-80s allowed for temporary advance, warming across the 20th century is the larger trend (Hanna et al. 2004).

While cool, cloudy summers and wet winters caused by the NAO have been associated with Icelandic glacier advance during the 20th century, these fluctuations are also seen as a semi-chaotic transition to the current warmer climate from cooler historical eras (Kirkbride 2002). Although the Icelandic Ice Sheet (IIS) was reduced in size from 60-25 kya (Andrews 2008), at the Last Glacial Maximum (LGM) the IIS covered most of Iceland with 2 km of ice and extended to the continental shelf break approximately 14 to 21 kya (see Figure 1.3; Hubbard et al. 2006; Licciardi et al. 2007; Norðdahl et al. 2008). LGM IIS volume was most sensitive to basal boundary conditions while areal extent was determined by bathymetry and calving activity (Hubbard 2006). After a series of advances and retreats associated with the Younger Dryas era ~10 kya, the mid-Holocene thermal optimum significantly reduced Iceland's glaciated area ~8 kya (Norðdahl et al. 2008).

Neoglaciation commenced 5-6 kya (Norðdahl et al. 2008), and despite advances bracketing the Medieval Warm Period in the 9th and 12th centuries (Kirkbride & Dugmore 2008), most Icelandic glaciers reached their Holocene maximum during the Little Ice Age (LIA; Flowers et al. 2007; 2008). Although the LIA climate shift appears to be synchronous across Iceland, depending on glacier size and type the associated advances were slightly offset (Kirkbride & Dugmore 2008). For example, although some small outlet glaciers saw their LIA maximum as early as 1700 (Kirkbride & Dugmore 2008), other lichonometric dating and tephrochronology studies show more common maxima in the late 18th and early 19th centuries (McKinzey et al. 2005b). Ethnographic research into areas such as decreased farming viability, more restricted population distribution, and decreased river usage also point to a glacial and climatic maximum of the Icelandic LIA in the late 18th and early 19th centuries (McKinzey et al. 2005a).

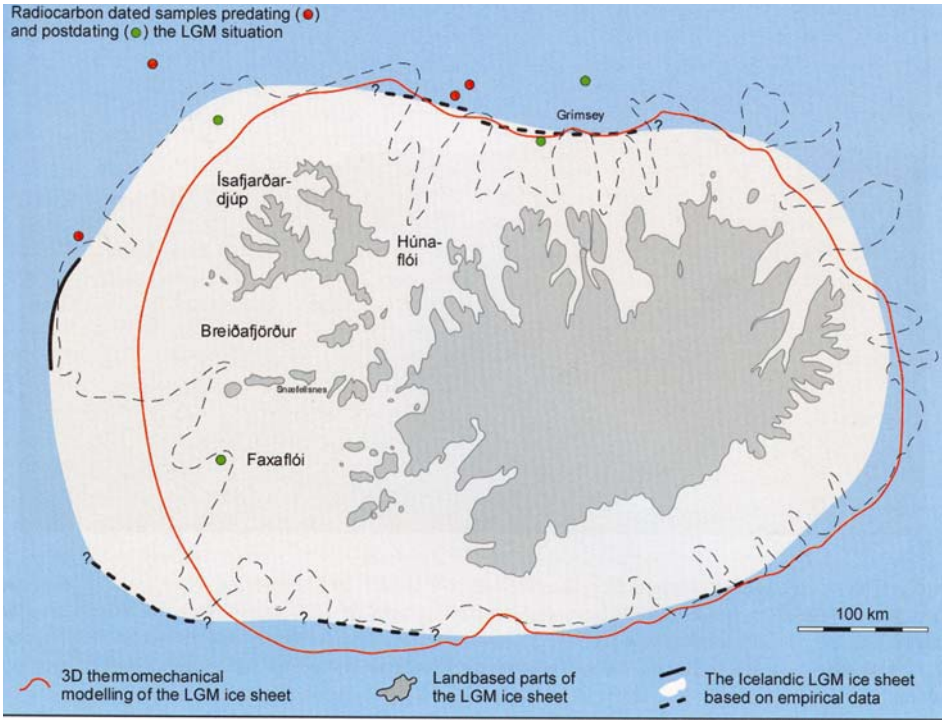

Figure 1.3 *Moraines and other physical evidence revealing the maximum size of the Icelandic ice sheet ~20 kya (Norðdahl et al. 2008); modeled and landbased outlines are according to Hubbard et al. (2006).*

In more recent times, a general recession of Icelandic glaciers over the past 200 years has been punctuated by slowing of retreat or even advance in the 1810s, 50s, 70s, 90s, and c. 1920 and 1970 (Sigurðsson 1998; Bradwell et al. 2006); Icelandic glaciers also fluctuated heavily in the 1930s and 40s (Bradwell et al. 2006). Although surge events often dominate a glacier's terminus, long-term recession of surging outlets, too, indicates a response to a warming 20th century climate (Magnússon et al. 2005). Many glaciers serve as good case studies of Icelandic climate change, but the most studied are the outlets of Iceland's largest icecap, Vatnajökull. Since the end of the 19th century, Vatnajökull has lost 10% of its mass, and this loss rate has accelerated in the last decade (Björnsson & Pálsson 2008); some lobes have retreated up to 2000 m in two decades (Williams et al. 1997), a result of a summer balance as large as -5 m.w.e. (Björnsson et al. 1998). Other studies have published figures such as a loss of 2.37 m.w.e. over 11 years (Björnsson et al. 2002), loss of 14 ± 5 km^3 from 1985 to 1998 (Magnússon et al. 2005), and retreat averaging 850 m over Vatnajökull's 130 km long perimeter (Magnússon et al. 2005).

Although not necessarily a synoptic view, measurements on Vatnajökull provide insight into the processes driving glacial fluctuations in Iceland. Summer temperature fluctuations, in particular, have been correlated with Icelandic glacial behavior; retreat in the 1930s was a response to warming in the 1920s, an advance beginning in 1970 corresponds to a cooling in the 1960s, and warming since ~1985 has led to an increased number of retreating

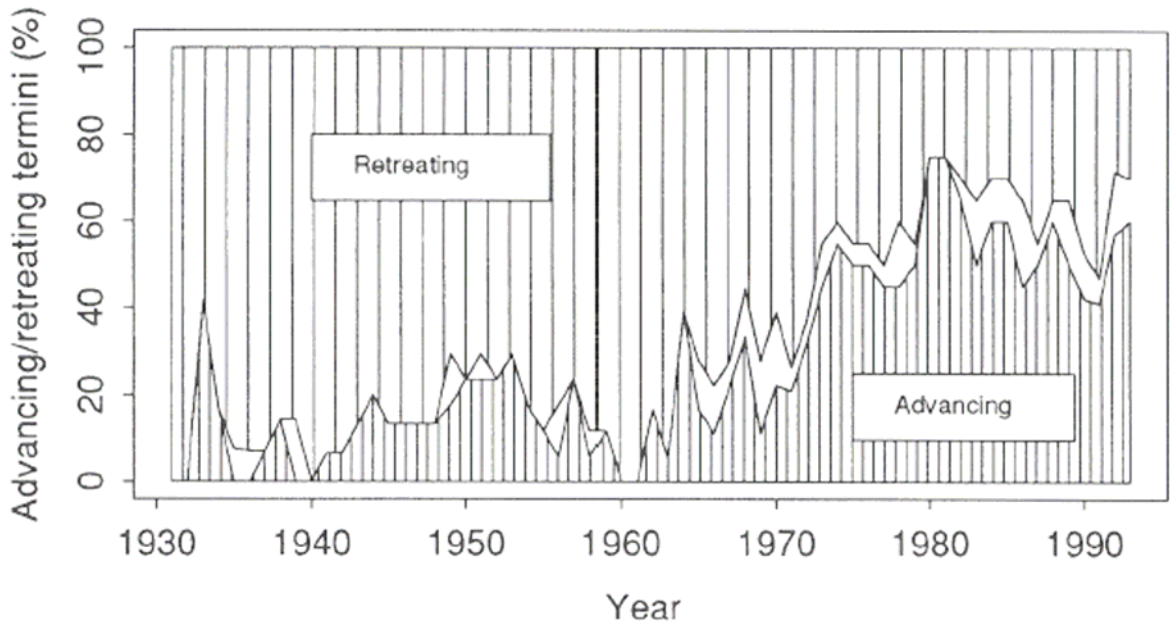

Figure 1.4 *Glacier fluctuation in Iceland 1930-1993; percentage of advancing and retreating non-surging glaciers relative to the total number of monitored glaciers (Sigurðsson & Jónsson 1995).*

glaciers beginning in the 1990s (see Figure 1.4; Sigurðsson & Jónsson 1995; Jóhannesson & Sigurðsson 1998). While winter mass balances have stayed fairly constant in recent decades, the summer balance, and hence annual net balance, has notably decreased from year to year (Björnsson et al. 1998).

This dramatic past behavior puts much speculation into the future behavior of Icelandic glaciers. While some studies suggest that icecaps such as Hofsjökull are near a stable equilibrium in a warmer climate, the much larger Vatnajökull is likely to lose at least 40% of its current volume before possibly stabilizing (Aðalgeirsdóttir et al. 2005; 2006). More pessimistic but still plausible models predict a 25 to 35% loss of the main Icelandic icecaps within half a century, leaving only small, isolated glaciers on high peaks in 150 or 200 years (Björnsson & Pálsson 2008). Whichever the case, advances in current monitoring knowledge and techniques will improve our understanding of the future behavior of the Icelandic icecaps.

1.1.1 Study Area

Langjökull (Icelandic for 'Long Glacier') is Iceland's second largest icecap (~950 km^2; maximum elevation ~1500 m.a.s.l.) and oriented SW-NE in central western Iceland (see Figure 1.5; Sigurðsson 1998). With an equilibrium line altitude at ~1000 m.a.s.l. and a low surface slope (<3.8 deg), Langjökull is thought to be a completely temperate ice mass; the widespread presence of moulins implies that melt water is freely able to reach the glacier bed (Eyre et al. 2005). The area is not volcanically active, there is no evidence for postglacial volcanic activity underneath Langjökull, and no recorded jökulhlaup has ever issued from

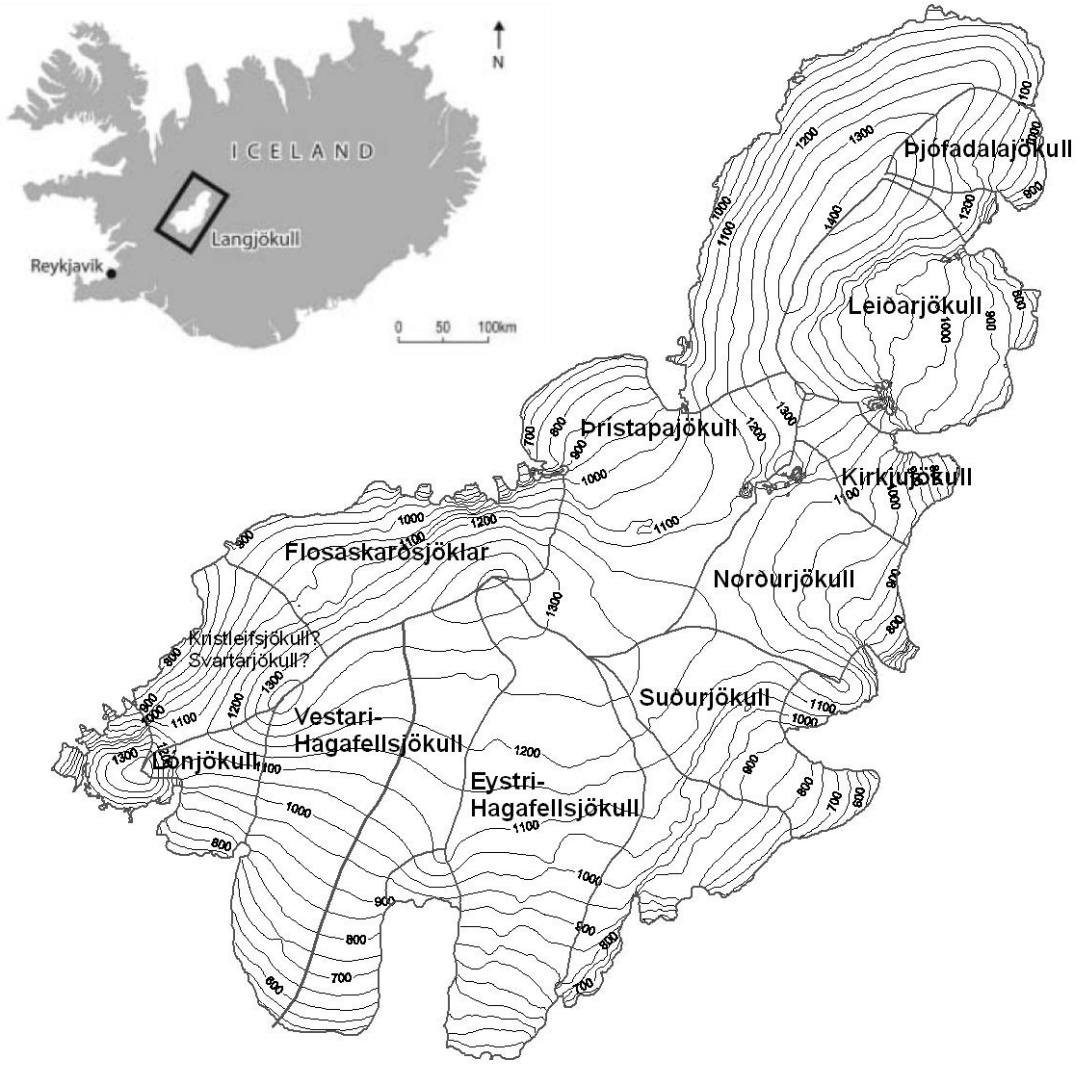

Figure 1.5 *Map of Langjökull including elevation (m.a.s.l.), ice divides, and central flowlines. In this study, Leiðarjökull is referred to as Jökulkrókur. Large map courtesy of Finnur Pálsson and Helgi Björnsson; inset from Eyre et al. (2005).*

Langjökull (Sigurðsson 1998).

The icecap itself has many outlet glaciers, two of which have historical records of surging behavior. On Langjökull's eastern edge, non-surge-type outlets Norðurjökull and Suðurjökull terminate in proglacial lake Hvítárvatn (Flowers et al. 2007) while Þrístapajökull is Langjökull's major western outlet. Jökulkrókur (also known as Leiðarjökull), in the northeast, has been monitored since 1933 along the valley Þjófadalir where it sources the river Fúlakvísl and has no known surging past (Sigurðsson 1998). In the south, the two major outlets, Hagafellsjökull Eystri and Hagafellsjökull Vestari are separated by the Hagafell Ridge. Both are surge-type glaciers believed to rest on a bed of deformable sediments (Eyre et al. 2005); Eystri surged in 1974, 1980, and 1998, Vestari surged in 1971 and 1980, and no previous surges are known for either glacier (Sigurðsson 1998; Bennett et al. 2005; Björnsson & Pálsson 2008). Hagafellsjökull Vestari is approximately 7 km wide, 25 km long, and

bounded on the east by the Hagafell Ridge. Hagafellsjökull Eystri is approximately 4 km wide and currently terminates in proglacial lake Hagavatn; constrained to the east by the Jarlhettur volcanic ridge, in places it overflows and forms small piedmont lobes in the Jarlhettukvísl Valley (Bennett et al. 2005). Past surges have formed complex deformation structures in and around lake Hagavatn (Bennett et al. 2000). During each surge Hagafellsjökull Eystri advances 1000-1500 m in late winter or early spring; in 1999 it first advanced 30 m in 24 hours, then 1165 m over the subsequent six weeks (Bennett et al. 2005).

Langjökull in its current state first significantly advanced 8.2 kya, remained quiescent throughout the mid-Holocene, and advanced again 3-5 kya (Flowers et al. 2008). Nevertheless, Langjökull's LIA maximum is thought to be its largest extent ever, sometime between 1840 (Flowers et al. 2007) and 1890 (Bennett et al. 2000). However, because many of Langjökull's outlets are quite stable, this maximum was still only ~10% larger in volume and ~5% larger in area than in the late 20th century (Flowers et al. 2007). While sufficient precipitation is thought to have been the most important factor for Langjökull's initial nucleation and growth, temperature has been it's most important driver since the LIA maximum (Flowers et al. 2008).

Termini of Langjökull have been scientifically observed since 1933; as is typical

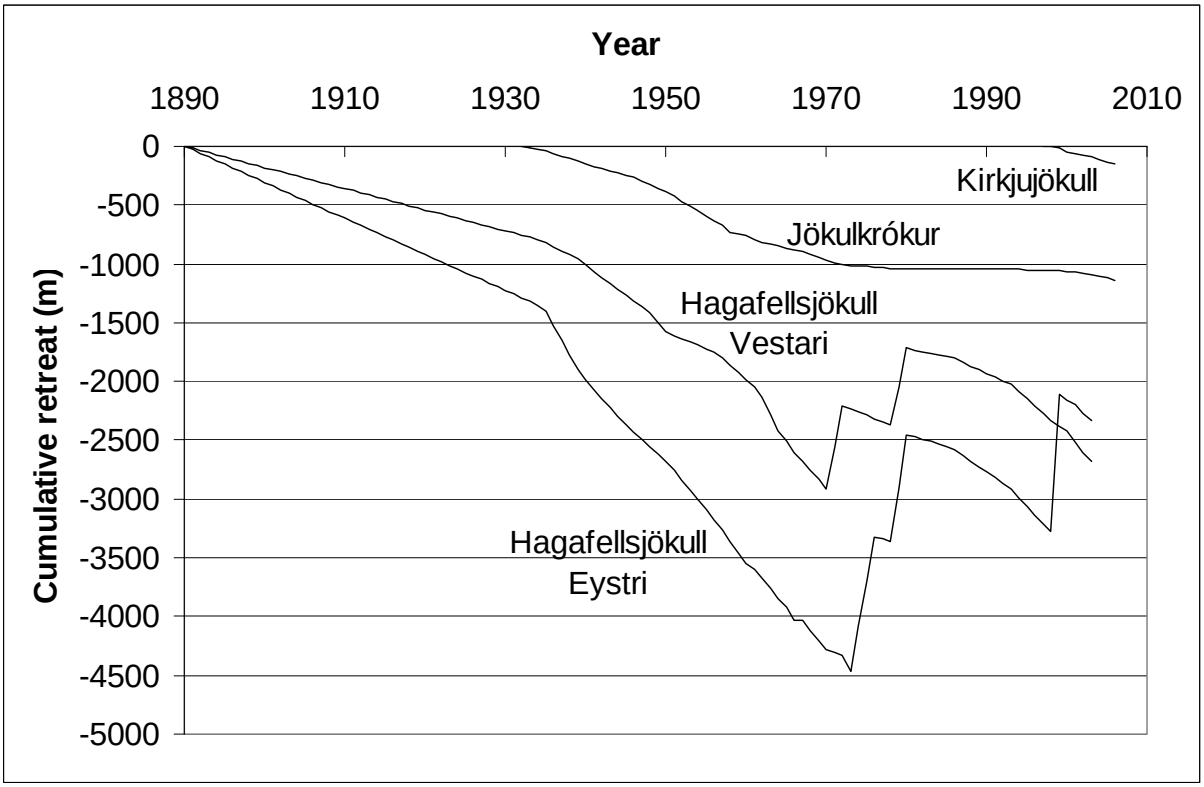

Figure 1.6 *Relative terminus location of four Langjökull outlet glaciers, with position 0 taken to be the beginning of the observational record for a given outlet. Note the large influence of surge events, as well as decreased negative slopes in the late 20th century. Data from Sigurðsson (1998; 2000; 2002; 2003; 2004; 2005; 2006).*

Iceland-wide, surge-type glaciers are dominated by their surge activities while on a whole there is a large retreat through much of the 20th century, with a slowing in the retreat beginning in the 1970s (see Figure 1.6; Sigurðsson 1998). From 1996 to 2001, Langjökull lost 5.73 m.w.e. or ~3% of its total mass (Björnsson et al. 2002), and the icecap is predicted to completely disappear around 2140 (Björnsson & Pálsson 2008). This loss is correlated with low snow accumulation and high annual temperatures (Björnsson et al. 2002); in order to conserve it's current state, Langjökull must experience increased winter precipitation and/or decreased annual temperatures (Flowers et al. 2007).

1.2 Studies of Glacier Topography

In Iceland and other study areas across the world, the construction of digital elevation models (DEMs) of ice surfaces is an essential application of remote sensing to glaciology (Barrand et al. 2009). Since the 1980s, satellite-derived data have been used to create DEMs of the continental ice sheets (Zwally et al. 1983). Technology has greatly progressed since then, and in current research, glacier DEMs are used as inputs for measuring mass balance via volume and areal change (Haeberli et al. 1999; Krabill et al. 1999; Rees & Arnold 2007), orthorectifying and processing images, delineating ice and water flow basins, and modeling ice mass flow (e.g. Joughin et al. 2009), energy balance (Arnold et al. 2006b), and mass balance at a point (Hubbard et al. 2000; Kääb & Funk 1999).

1.3 Glacial Topography Measurement Methods

Traditionally, a suite of techniques has been used to build glacier DEMs, ranging from ground-based theodolite survey and differential GPS transects to remotely-sensed satellite and airborne altimetry data. However, the desire for accurate, high resolution data over a large area is constrained by factors such as poor weather, time-intensive or expensive data collection, and challenging logistics. Satellite data is highly accurate over large areas, but the low horizontal resolution of altimetry data renders it unfeasible except for continental icesheets (Zwally et al. 2005). Therefore, either higher resolution visible light imagery or airborne collected data must be used for smaller ice caps and mountain glaciers.

Photogrammetry, a technique combining multiple photographs from different angles to create a three dimensional representation, takes advantage of high-resolution photography to build DEMs over glaciated areas (e.g. Kääb & Funk 1999; Barrand et al. 2009). However, photogrammetry relies on control points and high-contrast surfaces to co-register points in a stereo pair, which although feasible for melting glaciers (Rasmussen & Krimmel 1999) can

often be problematic in snow-covered regions (Krimmel 1999). Thus, although tractable, aerial photography is not an ideal method for remote glacier volume change measurements.

The technique of synthetic aperture radar (SAR) allows for airborne or spaceborne collection of images which are not subject to cloud-free or daytime conditions. However, SAR is unable to account for sudden topographical changes, and images often contain artifacts related to complex signal processing (p. 65-69, Rees 2006). SAR images can be used to distinguish between glacial regions (Demuth & Pietroniro 1999) and can accurately image glacial extent (Magnússon et al. 2005). By combining SAR images through interferometric SAR (InSAR), valuable DEMs can be created for determining changes in glacier elevation and extent (e.g. Björnsson et al. 2001; Magnússon et al. 2004) as well as measuring surface ice velocity (e.g. Guðmundsson et al. 2002; Rignot et al. 2008). However, care must be taken in assessing and correcting for the penetration depth of radar in order to ensure an accurate representation of ice and snow surfaces (Rignot et al. 2001; Berthier et al. 2006; Surazakov & Aizen 2006). Other applications of SAR data to build 3D data are radargrammetry (Simonetto et al. 1999; 2000) which combines stereo SAR images in a method similar to photogrammetry, and radarclinometry (Thomas et al. 1991; Pacquerault & Maitre 1998; Yang & Li 2003) which uses one or more SAR images to relate backscatter to surface slope in a method similar to photoclinometry, which is discussed in significant detail in Sections 1.3.2 and 3.1. For all uses, SAR images can be difficult and expensive to obtain and the data requires significant and complicated processing. Thus, while SAR is a valuable data collection method for building glacier DEMs, one must overcome significant logistical and scientific challenges to access its rewards.

1.3.1 LiDAR and Glacial Topography

Highly reflective glacier surfaces are very well suited to measurement by light detection and ranging (LiDAR). Also known as laser scanning, laser ranging, or laser altimetry, a LiDAR sensor emits a pulse of light and measures the time it takes for the pulse to reflect off a surface and return to the sensor. Then, it relates this two-way travel time to a distance based upon known signal velocity through the atmosphere. The exact position of the location measured by the pulse is then calculated based upon the location of the sensor and the direction it is pointed (see Figure 1.7); for airborne LiDAR sensors this is achieved with multiple differential GPS receivers and a gyroscope unit.[3]

[3] For a more technical description of the necessary corrections, see Favey et al. (1999).

Fortunately, glacial topography is in many ways ideal for airborne LiDAR use as the surface is not complicated by vegetation or drastically steep slopes. Indeed, because of the simplicity of the system, in addition to ranging capabilities, the strength of the LiDAR signal can be used to distinguish between rock, snow, and ice (Arnold et al. 2006a).

Figure 1.7 *Basic principle of LiDAR operation. In addition to the laser sensor, onboard the aircraft (the Dornier 228 pictured here was used to collect data for this study) are GPS receivers and a gyroscope unit used to precisely measure the location and orientation of the aircraft.*

LiDAR instruments are able to easily produce large amounts of data, which then must be efficiently dealt with. For DEMs, gridding points into a uniform matrix is considered the best practice. However, this interpolation is based upon the tenets that the terrain surface is continuous and that neighboring points are highly correlated (Liu 2008). Unfortunately, feature-specific points (i.e. peaks, valleys, ridges) are not generally well represented in gridded DEMs, although subsequent inclusion of these details often increases the accuracy of terrain representation (Liu 2008). Details of the processes used in this study are referenced in Section 2.1.

Like any method, LiDAR has its limitations. From any platform, satellite or airborne, LiDAR terrain measurements are impeded by interfering cloud cover, although in thin clouds data filtering can be used to salvage useful data (Arnold et al. 2006a). In addition, there is an inherent tradeoff between the area measured and the density of data collected by a given sensor (Rees 2006). Different platforms (ground-based, airborne, and satellite) each have independent considerations with respect to cost, time, data quality, and availability of sensors for data collection.

In research, deployment of LiDAR techniques is highly variable, including airborne profiling, airborne swath LiDAR, and a spaceborne sensor on the Ice, Cloud, and Land Elevation Satellite (ICESat). While ICESat measurements have a vertical accuracy of ~15 cm, measurements are also spaced over 170 m apart (Zwally et al. 2002), far too wide for small glaciers but perfect for large ice sheets. In addition to looking at behavior of continental ice sheets (e.g. Csathó et al. 2005), ICESat data have been used as inputs for ice sheet basal process models (Joughin et al. 2009). Airborne LiDAR, on the other hand, has been used to focus on smaller glaciers and icecaps. Originally restricted to profiles along glacier flow lines (Garvin & Williams 1993; Krabill et al. 1995a), introduction of swath LiDAR opened up

consideration of entire glaciers (Kennett & Eiken 1997). LiDAR has given insights into glacier evolution over the last half-century (Aðalgeirsdóttir et al. 1998; Sapiano et al. 1998), and current application of airborne LiDAR is used to look at short-term interannual glacier variability with very high resolution capabilities (Arnold et al. 2006a; Rees & Arnold 2007; Muskett et al. 2009).

Accuracy of LiDAR DEMs is based upon multiple factors including instrument calibration, sensor stability, navigation accuracy, and GPS accuracy (Krabill et al. 2002); advances in GPS technology have allowed for precise location determination and therefore correlation and combination of multiple data sets (Krabill et al. 2000). By comparing measurements of assumedly fixed features such as proglacial geomorphologic features and points where airborne flightlines cross LiDAR accuracy can be quantified (Latypov 2002). Profiling began with accuracies ranging from 50 cm (Garvin & Williams 1993) to 20 cm (Krabill et al. 1995b), and values in between (Echelmeyer et al. 1996). Current high-resolution methods reliably yield elevation to an accuracy of 10 cm on a 2 m grid (Rees & Arnold 2007).

1.3.2 Photoclinometry

Photoclinometry (PC; also known as shape from shading) is a method which unifies visible light imagery with elevation data. Put simply, PC transforms the brightness of a given pixel in a visible light image into a surface slope parallel to the solar azimuth for that image. Originally developed with regards to synthetic vision (Zhang et al. 1999) and planetary science (Howard et al. 1982; Kirk et al. 2003b), PC has become more popular in imaging Earth's surface, including sand dunes (e.g. Levin et al. 2004) and, more applicable to this study, polar regions. Studies have employed many different satellite imagers, both visible light and radiometric, to enhance already existing glacier DEMs (Scambos & Fahnestock 1998; Scambos et al. 1998; Scambos & Haran 2002), to use known tie points to build a DEM of a large area (Bindschadler & Vornberger 1994; Bingham & Rees 1999), and to investigate glacial features such as surface fractal dimension (Rees 1992), ice dolines[4] (Bindschadler et al. 2002), ice shelf streak lines (Raup et al. 2005), and ice stream dynamics (Scambos et al. 2004).

There are two general approaches in applying PC – an area-based approach which considers an image as a whole or a profile-based approach which integrates along parallel strips across the image. A profile approach (e.g. Bindschadler & Vornberger 1994) begins

[4] Ice doline – a depression formed on an ice shelf reminiscent of a sinkhole

with points of known elevation and builds off them in a direction parallel to sun azimuth. However, because there is effectively no consideration of cross-profile slopes, large errors can build up between adjacent profiles along integration lengths (Liu 2003). By contrast, area-based approaches take advantage of techniques such as Fourier transforms (e.g. Cooper 1994) or iterative minimization of an energy function (e.g. Hurt 1991; Liu 2003; Dulova et al. 2008) to relate slope in perpendicular directions. However, while scattered tie points can be used to attach an absolute elevation to a DEM generated by an areal approach, only profile integration is able to incorporate large numbers of tie points. In this way, area-based PC is able to fill in sparsely-constrained regions while profile-based PC takes advantage of more comprehensive elevation data sets which require augmentation.

1.4 Study Aims

This study is motivated by the desire to take advantage of a high resolution LiDAR data set (for details see Section 2.1) collected over Langjökull Icecap, Iceland. Due to logistical constraints, the aerial survey was left incomplete (see Figure 1.8); although coverage is largely continuous in the southeast quadrant, other areas are characterized by ~3 km strips lacking LiDAR coverage. Clearly, such a fragmented data set is not useful for glaciological applications. Therefore, the first aim of this study is to investigate the extent to which it is possible to interpolate elevations for the unmeasured areas using a combination of LiDAR tie points and a reasonably well established technique, photoclinometry. While employed in other circumstances to enhance or build relatively low resolution DEMs, here we seek to take advantage of the detail afforded by airborne LiDAR, evaluate suitable visual imagery for the task, develop a best practice for the technique, and build a final, complete, high resolution DEM for Langjökull. As with any technical investigation, there are inevitably new and unforeseen setbacks; we hope to assess these problems, overcome them, and evaluate the success with which we are able reconstruct icecap topography with photoclinometry.

Building on the product developed in the first part of this study will be a glaciological investigation of Langjökull. Through comparison of the LiDAR and PC-derived DEM with past DEMs, *in situ* mass balance data, and satellite imagery, this study will investigate changes in Langjökull over the past decade. In order to build a comprehensive portrait of the icecap, specific mass balance, spatial distribution of elevation changes, areal change, and margin advance and/or retreat will be interpreted. In particular, we will compare *in situ* and remotely sensed specific mass balance and investigate possible reasons for any observed discrepancies. Ultimately, the glaciological investigations in this study aim to afford a better

understanding of Langjökull's behavior in the recent past, what such observations likely mean for Langjökull's future, and how the icecap will continue to influence regional and global systems.

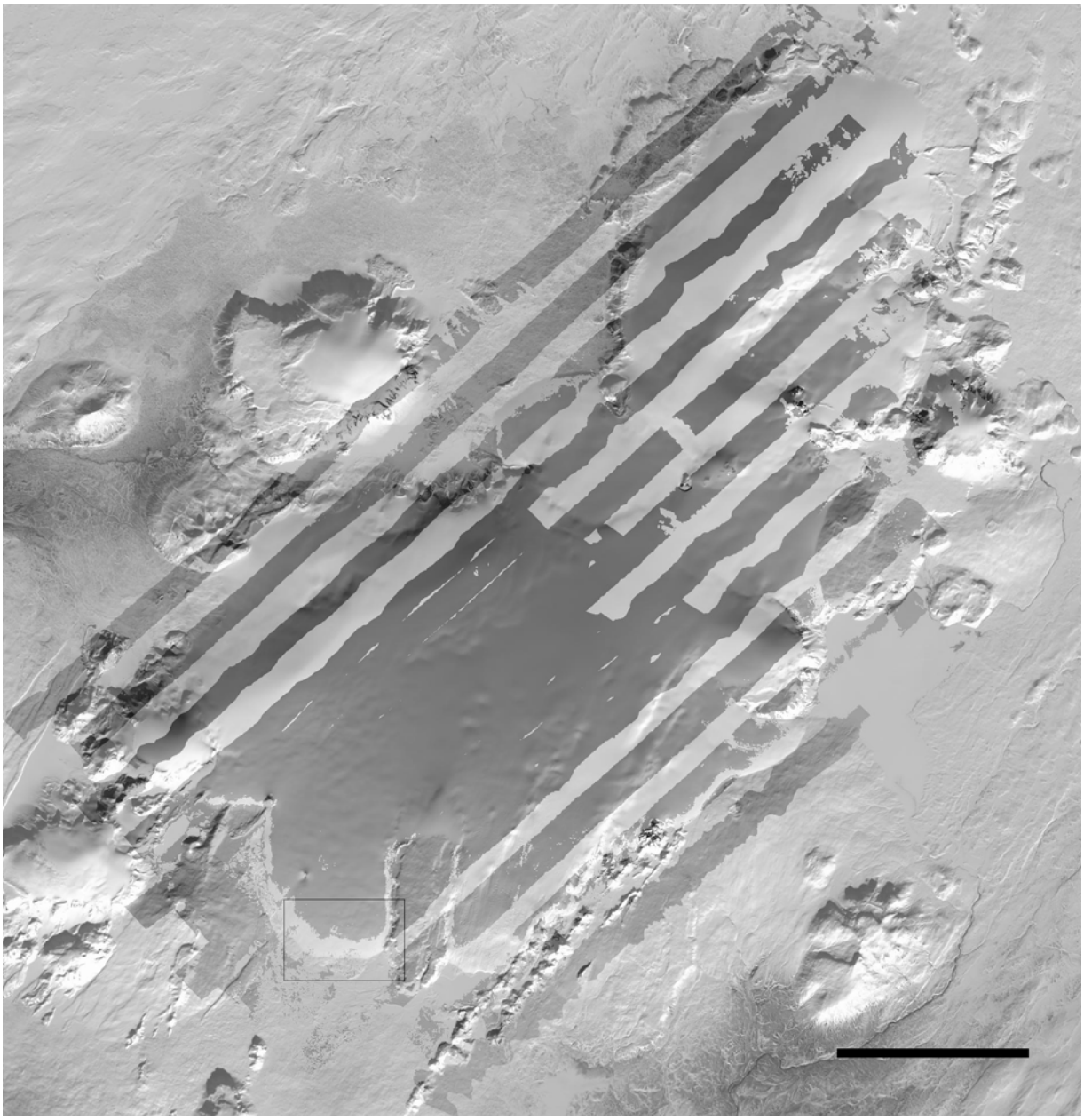

Figure 1.8 *Area of 2 August 2007 LiDAR survey masked over a 19 March 2002 Landsat-derived image. The rectangle indicates the location of the 2001 photogrammetrically-derived DEM of Hagafellsjökull Vestari (see Section 4.4). The scale bar is 10 km.*

2. Data Sources

2.1 Elevation Data

On 2 August 2007, an airborne LiDAR survey was flown for Langjökull (see Figure 1.8). The instrument used for data collection was an Optech ALTM3033 LiDAR system belonging to Cambridge University's Unit for Landscape Modeling flown aboard a Dornier 228 aircraft provided by the Airborne Research and Survey Facility of the UK Natural Environment Research Council. Details of similar acquisition and post-processing are given by Arnold et al. (2006). With a vertical accuracy of ~10 cm after processing, the DEM was accessed from an image file gridded to 10 m, 5617 pixels wide and 5795 pixels tall with the upper left corner at 510380E, 7201730N as plotted in UTM zone 27N with the WGS84 datum.

Additional summer 2007 elevation data were obtained via several differential GPS tracks collected on snowmobile and provided by Finnur Pálsson and Helgi Björnsson at the University of Iceland's Earth Science Institute. Differential GPS has ~2 cm vertical accuracy when sufficiently close to a base station. However, LiDAR and GPS data collection was not contemporaneous. After the tracks were gridded, comparison of areas of data overlap was undertaken to confirm that there was no systematic offset between the data sources. Demonstrating an almost normal distribution and thus no systematic bias, the absolute value of the offsets had a mean of 1.28 m and a root mean square error (see Equation 9) of 1.88 m. Because this error is less than predicted integration error (3.4 m, see Section 3.3.4), all supplementary differential GPS data were appended to the LiDAR DEM.

For temporal comparison, a DEM of the entire 1997 Langjökull surface and surrounding ice-free topography was processed by Ian Willis at Cambridge University's Scott Polar Research Institute from data again provided by Finnur Pálsson and Helgi Björnsson. Originally based on an extensive network of differential GPS snowmobile tracks, the Kriging method of interpolation was used to grid the data to 100 m and projected in UTM zone 27N.

Finally, as an intermediate between 1997 and 2007, a 2001 photogrammetrically-derived DEM based on 33 aerial photographs of Hagafellsjökull Vestari was provided by Richard Hodgkins at Loughborough University and Adrian Fox at the British Antarctic Survey. This DEM is gridded to 25 m with a vertical accuracy of better than 3 m and plotted in UTM zone 27N with the WGS84 datum.

2.2 Visible Imagery

In order to use PC to fill in the gaps in the 2007 LiDAR DEM of Langjökull, visible-light imagery of the entire icecap is required. Of course, resolution up the quality of the LiDAR

data (10 m) is desirable, but availability and cost must also be considered. Accordingly, imagery with 30 m horizontal resolution from NASA's Landsat program was chosen. A wide range of Landsat imagery is freely available by on-demand download through the United States Geological Survey's Earth Explorer service[5] and the University of Maryland's Global Land Cover Facility.[6]

Landsat imagery was required for two purposes: photoclinometry (PC) applications and an accurate delineation of Langjökull's complete terminus throughout the study period. Chosen based on the temporal constraint and the necessity for largely cloud-free images, see

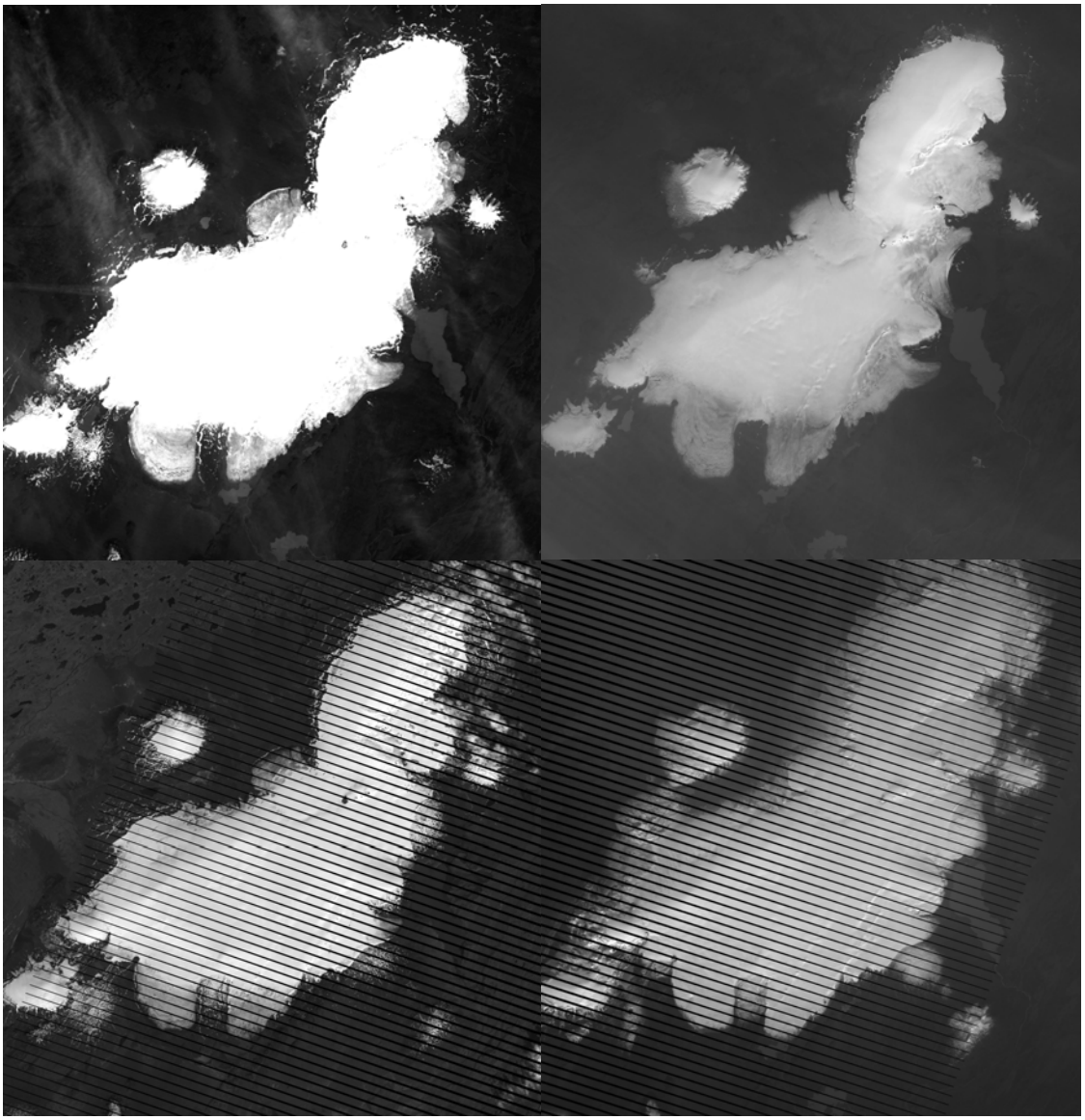

Figure 2.1 *Landsat images used for tracing Langjökull's areal extent: (upper left) Band 1, Landsat 5 TM, Path 219, Row 15 from 12 August 1994; (upper right) Band 1, Landsat 7 ETM+, Path 219, Row 15 from 8 September 2001; (lower left) Mosaic of Band 8 Landsat ETM+ Path 200, Rows 14 & 15 from 28 June 2007; (lower right) Band 1, Landsat 7 ETM+, Path 219, Row 15 from 25 September 2007. Note the gaps due to collection in SLC-off mode in the 2007 images (see Figure 2.2).*

[5] http://earthexplorer.usgs.gov
[6] http://glcf.umiacs.umd.edu/index.shtml

Figure 2.1 for the images from 1994, 2001, and 2007 employed here for visual identification of Langjökull's extent. The method of PC, however, imposes significantly stricter requirements on data which is employed. Obviously, cloud cover must be minimal, not only because clouds obstruct the surface, but shadowing by clouds also disrupts the homogeneity of reflectance necessary for PC (see Section 3.1). Care must be taken especially in distinguishing clouds which may be present over the ice surface but have a very similar albedo. Filters such as the Normalized Difference Snow Index can help in this identification (Hall et al. 1995a).

Related to the issue of homogeneity, the snow surface itself over the entire glacier must have uniform reflective properties. Summertime images will show a wide range of glacier surface types ranging from wet snow to glacier ice. Previous studies have determined that an early spring image allows for uniform snowcover without confounding hoar or ice patches (Scambos & Haran 2002). Ideally Landsat and LiDAR data would be collected contemporaneously, but these requirements over-constrain the available data. In order to allow for some compromise in selecting an appropriate data set, we consider first the variability in summer and winter small-scale topography, after which interannual variability in snowcover will be addressed in the context of glacier topography.

Snow-cover is known to be spatially inconsistent (Schneider 1999), and therefore does not exactly duplicate the underlying topography. As intuitively expected, consecutive LiDAR scans have shown on Alaska's Malaspina Glacier that concave areas fill with more snow than convex areas (Sauber et al. 2005), in most glacial cases due to wind redistribution of snow (Anschutz et al. 2007) thus producing a smoothed version of the underlying topography. In both flat (Shook & Gray 1996) and mountainous (Deems et al. 2006) environments, snow depth distribution is self-similar on small scales (<10 m) while essentially spatially-random on large scales (>30 m). For a given year, snowcover depth, and therefore the resulting springtime topography, are largely dependent on a complex mix of glacier aspect, microclimatological influences (Bamber et al. 2005), slope orientation (Lapen & Martz 1996; Richardson & Holmlund 1999), and altitude (Richardson & Holmlund 1999; Nuth et al. 2007).

In addition to intra-annual differences in glacier surface topography, there is considerable natural annual variability in local snow depths and accumulation rates (Bamber et al. 2005) which may in turn influence subsequent distribution of snow (Anschutz et al. 2008). Thus, while spatial distribution patterns of snow depth are often consistent, the snow depth at a given location varies considerably between years (Deems et al. 2008).

It is crucial to determine the scale of the effect that a different glacier surface will have on the eventual DEM that is produced with PC. One study using Landsat MSS data (60 m horizontal resolution) determined RMS error on it's elevation of 13.6 m (Bingham & Rees 1999). Interannual variations in glacier topography appear to be constant on the 5 m scale (Zagorski et al. 2008). High-resolution topographic studies have revealed surface variability on the scale of 7 cm a^{-1} in Antarctica (Anschutz et al. 2008), 2 m a^{-1} in Norway (Geist et al. 2005), up to 3 m a^{-1} in Svalbard (Nuth et al. 2007; Rees & Arnold 2007), and up to 10 m a^{-1} in temperate, maritime southeast Alaska (Cheshire 2008); variability appears to increase with the temperate nature of the glacier or ice sheet in question. Ultimately, any intra- or interannual glacier topographic variability should not be detectable via PC based on Landsat ETM+ as long as there has not been any surge activity between Landsat and LiDAR collection times. Therefore, rather than focusing on temporal proximity with LiDAR data collection, selection of imagery for PC processing is dependent on solar elevation, solar azimuth, and consistency of radiometric properties.

To greatly simplify computation, PC makes the assumption that the entire image is illuminated from the same solar elevation and azimuth. Therefore a single image rather than a mosaic of images is preferable. Once this Path/Row is found, it restricts the range in available solar positions, but ideally the elevation should be around 20º - low enough to cause variability in surface illumination, but not so low as to cause surface self-shadowing. In addition, because profiles are calculated parallel to solar azimuth, LiDAR swaths should ideally be placed perpendicular to the sun direction to minimize integration distance.

One additional consideration is a shift in the quality of Landsat data over the last decade. On May 31, 2003 the Scan Line Corrector (SLC) on Landsat 7, which compensates for the forward motion of the satellite during image collection, failed (Boloorani et al. 2008). Although the ETM+ continues to collect in SLC-off mode, approximately 22% of the image is missing with wedges of blank data spreading from 0 pixels wide in the center 22 km of the image (Wulder et al. 2008) to 14 pixels wide on the eastern and western edges of the image (see Figure 2.2; Maxwell et al. 2007). Nevertheless, the data collected in SLC-off mode is radiometrically correct and did not change any calibration levels (Markham et al. 2005). Many methods to

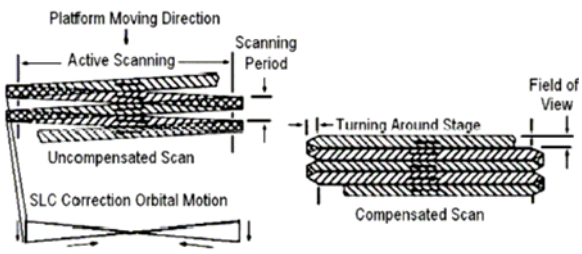

Figure 2.2 *Role of scanning mirror and SLC operation on Landsat 7 ETM+ (Reza & Ali 2008).*

restore missing data from SLC-off images have been tried, some quite successfully (Reza & Ali 2008; Roy et al. 2008; Wulder et al. 2008). However, computational methods (e.g. Schowengerdt 2007) are not sufficient for PC application, and contemporaneous supplementary data to fill in scan line omissions are unfeasible to obtain. Therefore, the complications introduced by post-SLC error data significantly outweigh any difference is Landsat data from a few years earlier which in fact introduce no additional error.

Based on all of the above considerations, a Landsat 7 ETM+ image from 19 March 2002 (Path 219, Row 15) was selected as the basis for PC augmentation of the 2007 LIDAR DEM (see Figure 2.3).

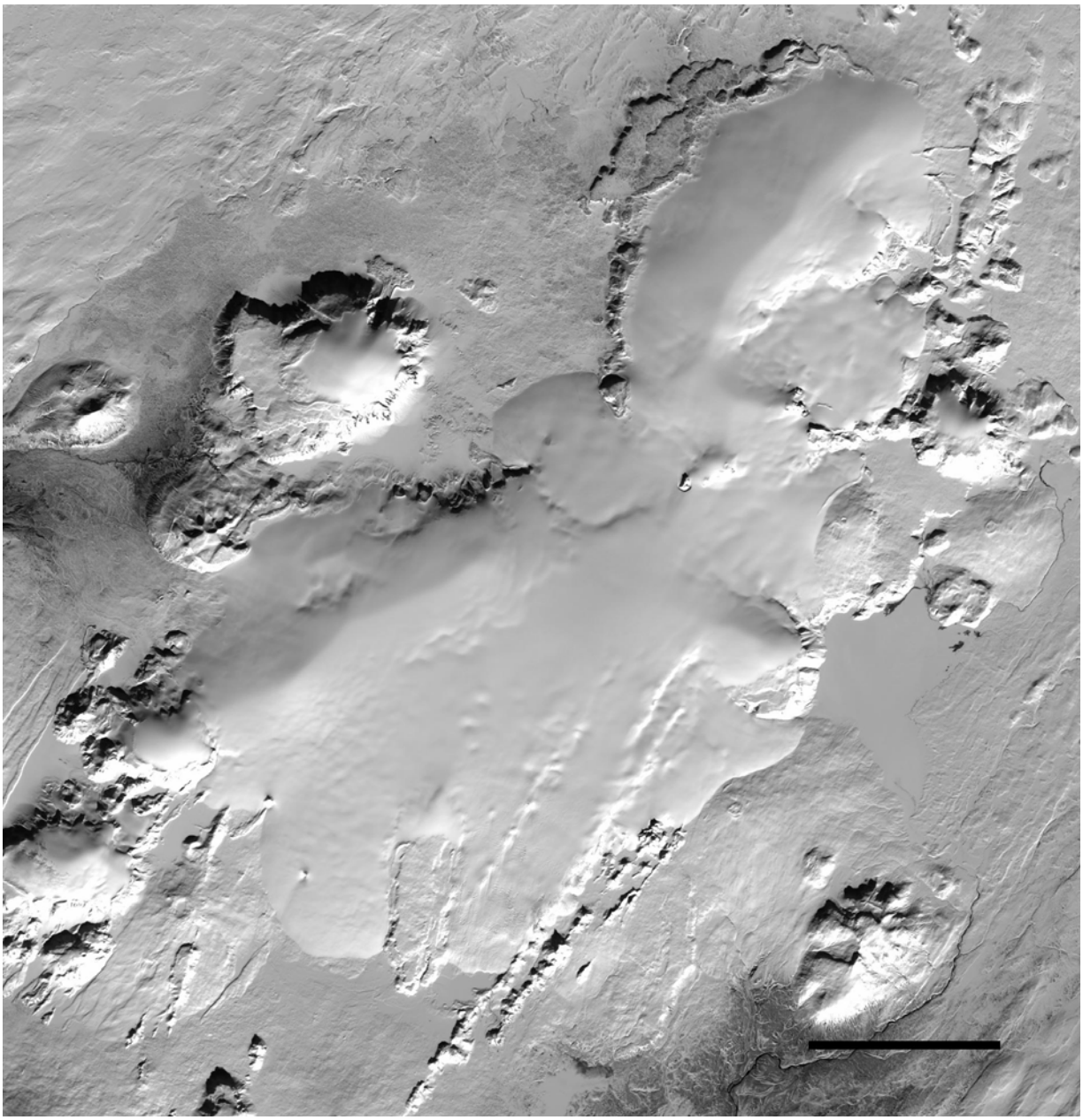

Figure 2.3 *Landsat ETM+ band 4 image (Path 219, Row 15) collected on 19 March 2002 used for PC interpolation in this study. Note that, as intuitively expected, icecap topography can be interpreted from image brightness. For more information on band 4 selection, see Section 3.3.3. The scale bar is 10 km.*

2.3 Mass Balance Data

In addition to the historical data documented by Sigurðsson (1998), and more recent monitoring efforts (Sigurðsson 2000; 2002; 2003; 2004; 2005; 2006), summer, winter, and net annual specific mass balances for Langjökull for the period 1996-1997 to 2006-2007 were provided by Finnur Pálsson and Helgi Björnsson at the University of Iceland's Earth Science Institute.

These data were collected using the stratigraphic method, measuring changes in glacier surface thickness and density relative to the summer surface in both the summer and winter across a stake network set up on many of Langjökull's outlet glaciers. The winter balance is estimated by drilling ice cores through the winter layer in the spring, and melt during the summer is measured from markers and snow stakes. A certain amount of variability is understood, for example resulting from drifting and redistribution of snow or predominant wind direction influencing precipitation, but elevation is the main variable determining position of sampling locations along flowlines and extrapolating from sample locations to the rest of the glacier. By combining stake measurements from multiple outlets, the final specific mass balance in theory accounts for both lateral and vertical variability in mass balance across the icecap. Error limits following integration are considered to be no lower than 15%.

3. Methods

While photoclinometry (PC) has been employed in a wide variety of situations and with many different types of elevation data and imagery, this is the first study which is based upon augmentation of very high resolution elevation data. As such, the considerations involved in combing LiDAR and Landsat ETM+ with easily available computing power are considered below.

3.1 Photoclinometry Theory

Intuitively, we know that visible-light images contain information concerning the topography they depict (i.e. see Figure 2.3); slopes facing towards the sun are naturally brighter than slopes facing away. Among other uses, on ice surfaces this basic understanding has been employed to identify ice divides (Dowdeswell et al. 1995). However, there are many assumptions and requirements which must be satisfied for PC to work properly (Kirk et al. 2003a). In particular, self-shadowed areas cannot be accurately imaged (Gelli & Vitulano 2004), and therefore a sufficiently large sun incidence angle is required; fortunately, ice sheet topography is usually subdued enough for this not to be an issue (Goodwin & Vaughan 1995). Solar incidence angles which are too high will saturate captured images while low angle light is complicated by increased atmospheric disturbance (Kirk 2003). In addition, the entire image is assumed to have the same reflective properties; following masking of any non-ice outcrops, this assumption has been determined to be valid for early-spring glacier surfaces that have not yet developed separate surface facies or hoar crystals (Scambos & Haran 2002).

In a more theoretically rigorous sense, PC use on glaciers begins with the assumption that snow is a Lambertian or diffuse reflector, scattering reflected light equally in all directions, rather than a specular reflector which reflects light only at an angle equal to the incidence angle (Zhang et al. 1999). Although snow is not a perfect Lambertian reflector (Warren 1982), for incidence angles above a couple of degrees, Lambertian behavior significantly outweighs specular reflectance (Choudhury & Chang 1981). Based upon a Lambertian reflectance model, image brightness can be described by

$$I(x,y) = \frac{\alpha \frac{\partial z}{\partial x} + \beta \frac{\partial z}{\partial y} + \gamma}{\left(1 + \left(\frac{\partial z}{\partial x}\right)^2 + \left(\frac{\partial z}{\partial y}\right)^2\right)^{1/2}} I_0 \qquad (1)$$

where the image brightness (pixel value, *I*) is a function of the Cartesian components of the unit vector in the direction of solar illumination (α, β, γ), the Cartesian coordinate of the surface (*x* and *y* horizontal, *z* vertical), and I_0, the image brightness for a normally illuminated pixel (Cooper 1994; Bingham & Rees 1999). For this to be a valid relation, it is important that image brightness not be saturated (Cooper 1994). This general equation is simplified by assuming that the surface slope is small such that

$$1+\left(\frac{\partial z}{\partial x}\right)^2+\left(\frac{\partial z}{\partial y}\right)^2 \approx 1 \tag{2}$$

This simplification is valid for low slope areas; a later section (see Section 3.3.2) evaluates this assumption for Langjökull. In addition, we establish a Cartesian coordinate system whereby the *x*-axis is parallel to the solar azimuth, thereby causing β to be 0. Implicit in this simplification is the assumption that both sun and satellite imager are distant enough that the entire image can be described by constant incidence angles and solar azimuth. Based on these two simplifying assumptions we are left with the following:

$$I(x)=\alpha'\frac{\partial z}{\partial x}+\gamma' \tag{3}$$

where $\alpha'=\mathrm{I}_0\alpha$ and $\gamma'=I_0\gamma$ (Bingham & Rees 1999).

Equation 3 shows that for a Lambertian surface, slope and image brightness should be linearly related. Image brightness and surface slope were first shown to be linearly related by Rees and Dowdeswell (1988). Likewise, other studies show a similar relation (Scambos & Fahnestock 1998) whereby:

$$I=A\cos\theta+B \tag{4}$$

in which $A=CUR$ and $B=C(T-L_0)$ where *C* is the constant of conversion from radiance units to sensor units, *U* is the incident illumination at the surface, *R* is the reflectivity, θ is the angle between the surface normal and the solar incidence vector, L_0 is the minimum radiance threshold for the sensor, and *T* is the radiance at the sensor from all sources other than the surface, such as atmospheric scattering.

By using areas of overlap between visible imagery and a pre-existing DEM, the relationships in Equations 3 and 4 can be investigated and the Lambertian assumption evaluated (i.e. a linear relationship confirms validity of the method). In the case that slope and brightness data cannot be compared, it may be possible to employ dark pixel values and assumptions about low surface slope in order to quantify the constants in Equation (Bindschadler et al. 2002). In this study, see Section 3.3.3 for application of Equation 3.

Based on known tie points and a calculated surface sun-parallel slope, it is possible to interpolate the intermediate topography. All LiDAR data are treated as correct representations of the surface, and Landsat-based interpolations are fitted within this framework. Starting from Equation 3, we rearrange the expression such that the slope is expressed as follows:

$$\frac{\partial z}{\partial x} = \frac{I(x) - \gamma'}{\alpha'} \tag{5}$$

where α' and γ' are empirically derived according to Equation 3. Before further progression, the expression must be discretized such that it is compatible with raster data.

$$\frac{\partial z}{\partial i} = \frac{I(i) - \gamma'}{\alpha'} \tag{6}$$

where i is the pixel count and p is the width of one pixel such that $x = ip$. In this discretized frame, the elevation of a point can be calculated if the elevation of the adjacent point in a sun-parallel direction is known:

$$z(i) = z(i-1) + p\frac{\partial z}{\partial i} \tag{7}$$

Simple substitution with equation 7 yields the final expression:

$$z(i) = z(i-1) + p\frac{I(i) - \gamma'}{\alpha'} \tag{8}$$

Iterated for each subsequent unknown point, gaps between known tie points can be easily interpolated or unknown perimeter values can be extrapolated if desired, although the latter is discouraged for multiple reasons including the fact that the coefficients are likely to be different for differing surfaces. Finally, for interpolated topography a linear scaling measure is taken to ensure that calculated values are consistent with tie points on both sides of a void.

It should be noted that here we integrate in a sun-parallel direction for simplification of computation and because it is in this direction where slope information is stored (Liu 2003). However, combinations of multiple images have been used in reconstructing planetary surfaces to account for variable albedo (Lohse et al. 2006). In terrestrial polar applications, combining images with solar azimuths close to 90º apart has been employed to gain slope information in multiple orientations (e.g. Scambos et al. 1998; Raup et al. 2005). However, this method requires intensive cross registration of images to within one pixel accuracy so that precision is not lost, a technique which is very difficult on surfaces such as ice where there is very little contrast. Ultimately, obtaining multiple cloud-free Landsat images for this area with appropriate temporal proximity is unfeasible.

3.2 Software Methods

An important consideration in dealing with remote sensing data is how to approach computational tasks. There are many software packages available, and each has its specialty, whether speed, power, or ease of use. For this project, Multispec 3.1[7] was used for simple Landsat data processing, ImageJ 1.42i (64-bit)[8] was used for image analysis and visualization, ERDAS Imagine 9.0 was used for more complex GIS tasks, and MATLAB R2008b was used for complex computation, specifically treating gridded elevation image files as large matrices.

3.3 Photoclinometry in Practice

In this section, the assumptions inherent in photoclinometry are shown to be valid for this data set, and the practice of filling in the gaps in the 2007 LiDAR DEM is elaborated upon.

3.3.1 Image Processing and Interpolation

As mentioned above, ImageJ 1.42i (64-bit) provided an easy and efficient software tool for handling images. The "scale" feature in the software was used to match up the LiDAR, gridded at 10 m, and the Landsat images which have a resolution of 30 m. Similarly, for later integration in a sun-parallel direction, the "rotate" feature was used to realign all images from standard format, with north as up, to sun-parallel as up; sun azimuth as well as other information pertaining to the conditions of the Landsat image in question is available in image header files provided with the multispectral imagery.

Because this study integrates many different data sets from various sources with diverse levels of spatial resolution, careful consideration was required in deciding the appropriate method to unite the data into cogent, cohesive, and convincing results. At one end of the spectrum is the airborne LiDAR gridded to 10 m, which is an order of magnitude more detailed than the 100 m gridding of the 1997 DEM; the visible Landsat imagery is provided at an intermediate 30 m horizontal resolution.

Attempting to interpolate the 1997 up an entire order of magnitude would introduce many concerns and also falsely induce an increased sense of spatial detail. However, it would be unfortunate to dispose of large amounts of new and valuable LiDAR data. Rees (2000) finds that simple bilinear interpolation is more than adequate for increasing DEM resolution with error increased by only 0.2σ to 0.6σ. Therefore, a middle ground of 30 m was chosen as the common resolution for comparison of all data sets. For this task, bilinear interpolation is

[7] Multispec is freeware available from http://cobweb.ecn.purdue.edu/~biehl/MultiSpec/
[8] ImageJ and associated plugins are freely available at http://rsbweb.nih.gov/ij/

employed because it is computationally simple and does not introduce outlying values into the data set.

Once at a common resolution, in order to preserve data as closely as possible to their original form, nearest-neighbor interpolation was consistently used. Various small tests showed that nearest-neighbor interpolation produced data of a similar quality to other methods such as bilinear interpolation without resulting in problematic edge effects when areas of no data were averaged with pixels containing elevation data.

3.3.2 Validating the Low Slope Assumption

In order for brightness to be linearly related to surface slope, the terrain must be of sufficiently low slope to allow for the mathematical simplification that

$$1+\left(\frac{\partial z}{\partial x}\right)^2+\left(\frac{\partial z}{\partial y}\right)^2 \approx 1 \qquad (2)$$

While polar icesheets and icecaps typically have surface slopes below 3º (Bingham & Rees 1999), the more temperate and maritime nature of Langjökull does draw this assumption into question. While low slopes are ideal, increased slopes are still tractable with PC but introduce a larger error in elevation determination; a 25º slope corresponds to a 10% error in elevation determination along that slope (Cooper 1994). Still, useful results have been achieved with slopes as high as 30º (Cooper 1994).

Accordingly, the sun-parallel slope of the available LiDAR imagery was calculated for the entire icecap. There are many areas of moderate to high relief (>10º), but based upon visual inspection these are largely ice-free areas not involved in the PC calculations. Nevertheless, Langjökull is a fairly smooth icecap with a mean slope of 7.5º as calculated from available LiDAR data. Thus, although not as ideal as many less temperate icecaps, it is determined that the Langjökull is an acceptable location for the application of PC.

3.3.3 Validating and Optimizing the Slope-Brightness Relationship

Equation 3 shows that Landsat brightness and LiDAR slope must be related in order for PC to perform satisfactorily. In addition to using this relationship to validate the Lambertian assumption, because of the multispectral nature of Landsat data, we also use the linear slope-brightness relationship to select the best subset of data to use for PC interpolation. In this case, the best band or band combination to use in relating brightness to slope is measured by the R^2 goodness of fit parameter.

First, the histogram of each possible image was reviewed to ensure that the image was not overly saturated or insufficiently contrasted, both situations which would limit the amount and range of topographic information stored by the brightness. With this initial consideration in mind, bands 1, 2, 3, 4, 5, 7, 8, the first principle component,[9] and band combinations 123, 234, 124, and 134 were tested for a linear relationship between sun-parallel slope and brightness. In order to ensure a feasible test, and in order to have the highest likelihood of using fresh, dry, unmelted snow, a 4 km x 4 km square of data was sampled as close to the center of the icecap as possible where LiDAR data was continuous.

R^2 values were as low as 0.12 (band 7), and many fell around 0.4 (first principle component, band 3, all band combinations), but band 4 brightness values best fit a linear correlation with the LiDAR-based slope values (R^2=0.45). This is expected, as past studies have also used Landsat band 4 for PC (Bindschadler & Vornberger 1994; Bingham & Rees 1999). While this goodness of fit is significantly below some published values (e.g. 0.84, Bingham & Rees 1999), it is more important to verify that there is no spatial pattern to the distribution of residuals and to investigate the accuracy with which PC based on Landsat band 4 can reproduce known topography before interpolating unknown values.

Areas of slightly increased topography were found to correspond to higher residuals, but without any systematic pattern of over- or underestimation. It is likely that the low R^2 value is a result of higher slopes on Langjökull compared to previous studies based on High Arctic icecaps and the Antarctic Ice Sheet. In addition, uncertainty in the brightness-slope relationship is the result of variations in albedo as well as the surface's bi-directional reflectance distribution function (BRDF) caused by inhomogeneity of surficial properties such as roughness and snow grain size (Bingham & Rees 1999). Indeed, regression with a smaller subset of data resulted in R^2 values as high as 0.8, however higher R^2 values were also paired with a lower reproducibility of coefficients.

Reproducibility and lack of bias in regression is key because one set of coefficients from Equation 3 will be used in Equation 8 and ultimately applied to the entire 2007 DEM. Because properties such as sensor orientation and sunlight incidence angle are taken to be constant across the entire image, we test for bias in individual sun-parallel profiles 6 km long moving across the image; there was no observable trend in the sun-perpendicular direction across the icecap, therefore we assume that generalizations across the entire image are valid.

[9] First Principle Component: The result of an orthogonal linear transformation which displays the greatest variance by any projection of the data. In this way we try to harness the common points of all reflective Landsat bands while removing the variation between them.

In addition, because the Landsat imagery was collected in early March, it is possible that some melting had begun which would potentially cause the albedo and BRDF to vary depending on location within the icecap. However, based on a series of 2 km x 2 km squares of data starting on the high ice divide and moving to the tongue of Hagafellsjökull Vestari, there is no trend in the linear relationships between slope and brightness. Therefore, based on the above tests, it is determined that a global set of coefficients for Equation 3 is appropriate.

At this point it is necessary to determine which coefficients will be used for PC calculations. Although one set of α' and γ' will be used for the entire image, using the entire set of available data to determine the coefficients results in very low correlation values ($R^2 <$ 0.1). This result is not surprising, as this method does not eliminate areas of high relief or saturation. Alternately, areas of high correlation are not identifiable upon simple inspection. Therefore, the largest area of continuous data in flat, high ice areas is identified and used to determine that $\alpha' = -357.7816$ and $\gamma' = 185.9914$. These values are used in the rest of this study for interpolation of glacier surface topography.

3.3.4 Integration and Error Assessment

Before applying PC to completion of the 2007 Langjökull DEM, especially considering mediocre correlation between brightness and slope, it is important to test reconstructions of known profiles and areas. In order to assess the error in the method and quantify confidence in PC, we use the root mean square (RMS) error as a metric for identifying the quality of topographic reconstruction.

$$Error_{RMS} = \sqrt{\frac{1}{n}\sum_{i=1}^{n} e_i^2} \tag{9}$$

where here e is the difference between PC-interpolated and LiDAR-measured elevations. In addition to the quantified RMS error, we look at the accuracy of reproduction of topographic lows and highs, consistently misrepresented features, and/or any extreme or unrealistic values.

Table 3.1 shows error information for 3 km and 6 km long sun-parallel test profiles selected from across Langjökull's entire surface; the 3 km profiles are simply the first and second halves of the 6 km, but with an added tie point in the middle. Despite a wide range of RMS errors, 0.3 m over 3 km to 19 m over 6 km, topography is quite well reproduced (see Figure 3.1). Although past studies have suggested that error increases linearly with integration distance (Bindschadler & Vornberger 1994), we find here that in most cases (with the notable exception of profile 2) the error does not rise proportional to integration distance.

Table 3.1 *Error calculated from test profiles of photoclinometric interpolation in areas of known topography.*

Test	Dimension	RMS error (m)
Profile 1.0	6 km	5.12
Profile 2.0	6 km	19.00
Profile 3.0	6 km	10.74
Profile 4.0	6 km	5.67
Profile 5.0	6 km	12.46
Profile 6.0	6 km	0.41
Profile 1.1	3 km	3.12
Profile 1.1	3 km	2.62
Profile 2.1	3 km	6.08
Profile 2.2	3 km	1.32
Profile 3.1	3 km	5.20
Profile 3.2	3 km	5.36
Profile 4.1	3 km	0.85
Profile 4.2	3 km	3.28
Profile 5.1	3 km	9.63
Profile 5.2	3 km	10.75
Profile 6.1	3 km	0.29
Profile 6.2	3 km	0.38
Area 1	3 km x 3 km	3.73
Area 2	3 km x 3 km	2.70
Area 3	3 km x 3 km	3.74

Significantly, there does not appear to be any bias with respect to over or underestimation of absolute elevation or slope. Indeed, it is quite possible that due to interannually variable processes such as snow drifting the topography from the Landsat image is in fact not quite identical to the LiDAR topography. However, close correspondence confirms that it is an acceptable substitute.

Area integration, that is a series of parallel profiles, is the next logical and required step for successful DEM completion. For final DEM production, MATLAB protocols were written for identifying and interpolating topography for areas of unknown data of all sizes within the LiDAR data set. However, for this testing purpose we focus on reproducing known areas with standardized areas of interpolation. Because PC represents topographic data only in the sun-parallel direction, large inaccuracies of cross-sun slope can build up along the integration of adjacent profiles (see Figure 3.2). Because these cross-sun slopes are outside the distribution of small scale surface slopes, they are believed to be artifacts rather than an accurate representation (Bindschadler & Vornberger 1994).

To remedy this problem, past studies have used a cross-slope running average of sun-azimuthal slopes to remove unrealistically large slopes. However, this is effectively equivalent to smoothing the original Landsat data, which is undesirable in creating an accurate, high resolution DEM. Instead, this study suggests the use of a cross-sun running average of PC-interpolated elevations to remove such artifacts. Using examples where just one profile was interpolated and one of an entire area of interpolated topography, running averages of 3, 5, 7,

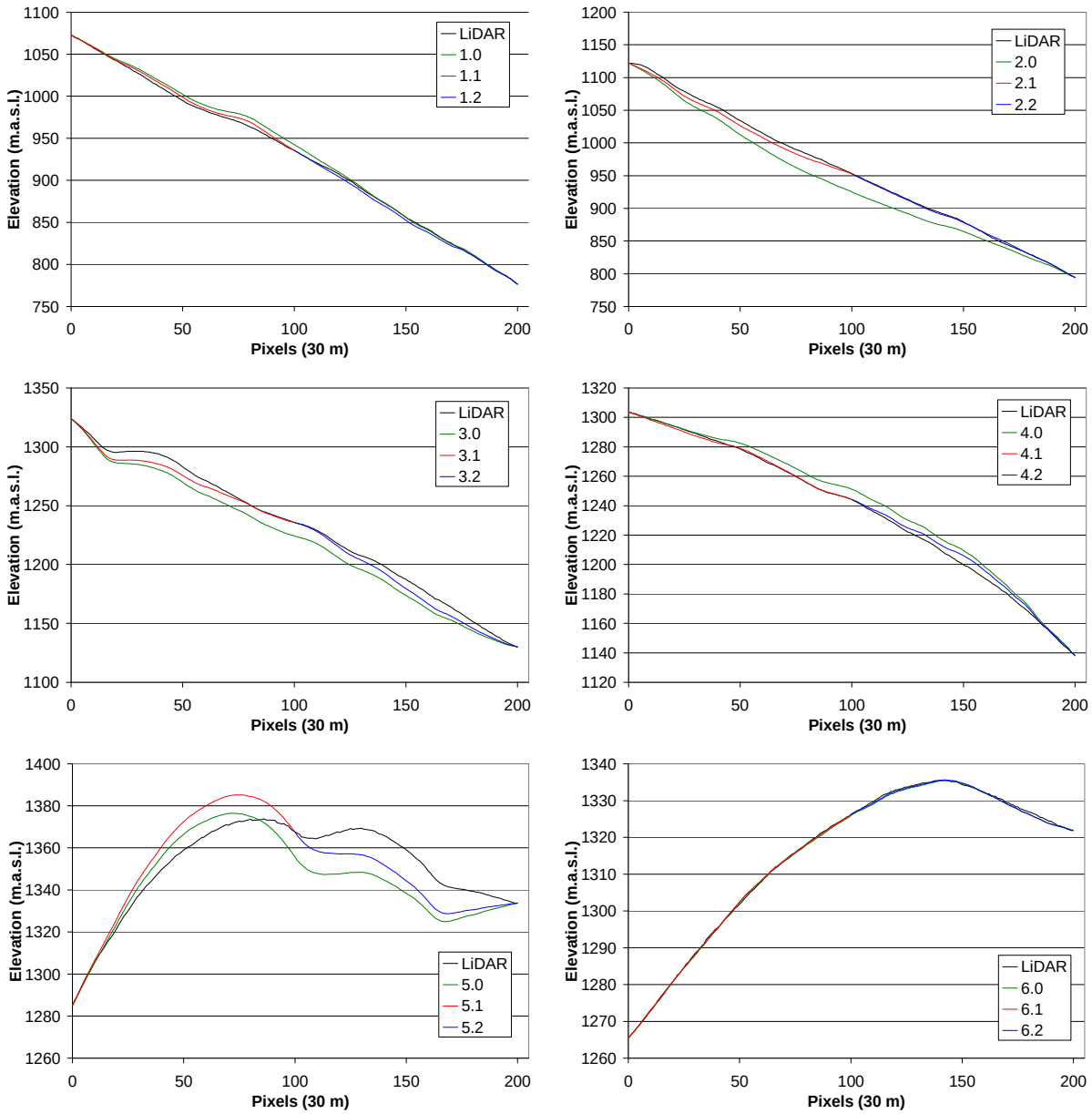

Figure 3.1 *Comparison of photoclinometric interpolation and LiDAR-measured profiles. Each graph contains one LiDAR profile, a 6 km profile tied by one LiDAR data point at each end, and two 3 km profiles, each tied by one LiDAR data point at each end.*

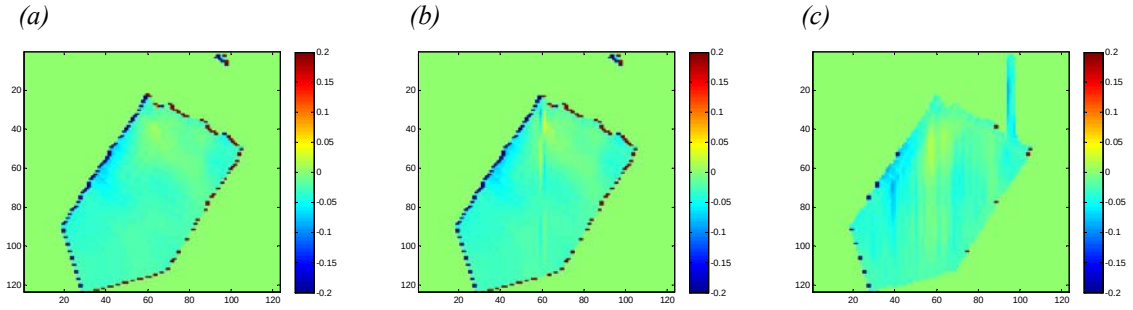

Figure 3.2 *Comparison of cross-sun slopes in (a) LiDAR-measured elevations (b) LiDAR-derived elevation with one PC-interpolated profile and (c) PC-interpolated elevations. Note the higher values and vertical artifacts present in (b) and (c). Both x- and y-axes are measured in 30 m pixels. The pentagon shape is a result of extraction from the LiDAR DEM; all values outside of this perimeter contain no data.*

and 9 pixels were tried (see Figure 3.3). It is worth nothing that this smoothing will be of varying importance for eventual uses of the PC-interpolated DEM; while studies such as entire icecap volume change will not be changed, high resolution studies will by slightly influenced by regional averaging. Based upon visual inspection, a running average of 5 pixels, in this case 150 m, provides a balance between reducing DEM resolution and eliminating vertical artifacts in order to make the topographic reproduction more realistic. Following smoothing, original LiDAR values are replaced so that, effectively, only interpolated values are averaged.

Using this 5-pixel running average as a post-PC step, the topography of three known 3 km x 3 km areas from upper, middle, and lower glacier areas was reconstructed as a final test to asses the error of PC reconstruction. The size of the square was chosen to approximate the length of an average integration in final DEM interpolation. While LiDAR-derived elevations remain accurate to within ~10 cm, based on the above area reconstructions and previous 3 km profiles, the RMS error in elevation of PC-derived values is determined to be 3.4 m.

3.3.5 Final DEM Construction

The methods above provide the details for augmentation of the otherwise incomplete airborne LiDAR survey of Langjökull. However, the extent of LiDAR tie points does not allow for complete coverage of Langjökull via photoclinometric interpolation, in particular the northern section of the icecap. Therefore, a profile of tie point elevations in non-ice covered areas slightly north of the icecap was taken from the 1997 DEM in order to provide a complete view of Langjökull in summer 2007.

There should be very little difference in elevation of non-ice covered areas between 1997 and 2007; to verify, however, 32 points of overlap between the added points and the LiDAR DEM were compared. The residuals approximately normally distributed, showing no systematic bias to over- or underestimation; with a mean absolute error of 5.5 m, the agreement is not ideal but is much preferable to excluding a portion of Langjökull. As such, the very northern section of the DEM will be regarded with caution and carefully critiqued in the discussion of results not only because 1997 data was used for a 2007 DEM, but also because this solution requires the use of PC on snow covered rock rather than only glacier surface, a process not optimized in DEM construction procedures.

The final DEM produced of Langjökull's entire summer 2007 surface (see Figures 3.4 and 3.5) based on LiDAR and Landsat data is gridded to 30 m horizontal resolution. The test

Figure 3.3 *Comparison of cross-sun running averages. The pentagon shape is a result of extraction from the LiDAR DEM; all pixels outside of this perimeter contain no data. Images in the left-hand column (a-e) are the difference between PC-interpolated elevation after cross-sun smoothing and known LiDAR elevation. Images in the right-hand column (f-j) are cross-sun slopes calculated after running average smoothing. Both x- and y-axes are measured in 30 m pixels. A 5 pixel running averaged was determined to be a good balance between eliminating vertical artifacts and over-smoothing data.*

(a) Residual; no running average

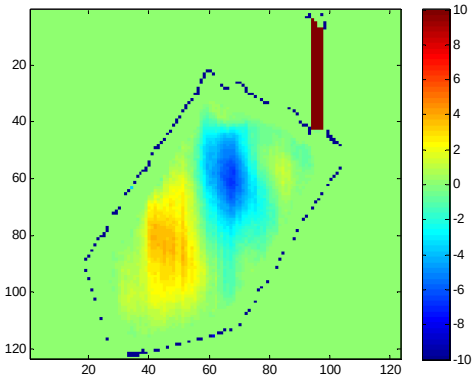

(f) Cross-sun slope; no running average

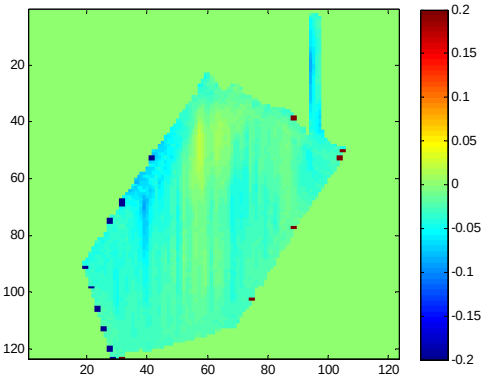

(b) Residual; 3 pixel running average

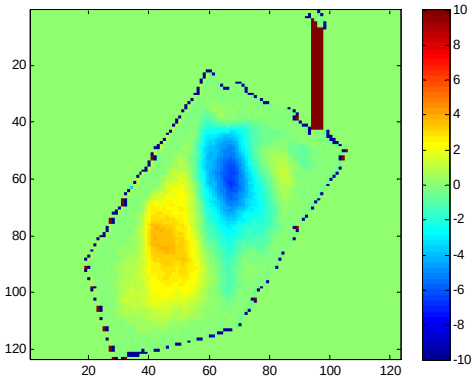

(g) Cross-sun slope; 3 pixel running average

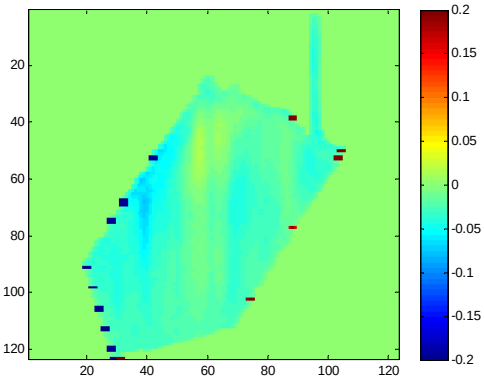

(c) Residual; 5 pixel running average

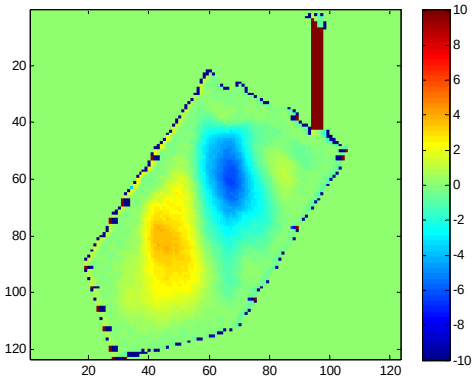

(h) Cross-sun slope; 5 pixel running average

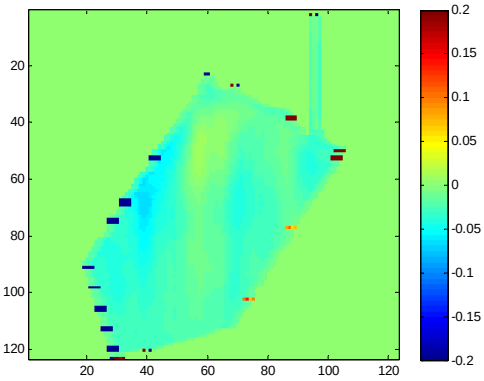

(d) Residual; 7 pixel running average

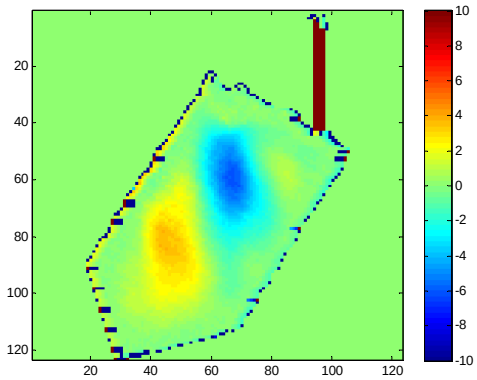

(i) Cross-sun slope; 7 pixel running average

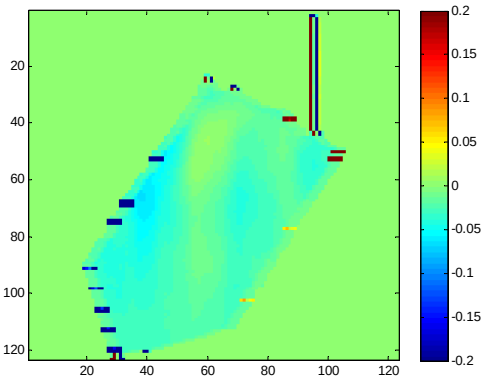

(e) Residual; 9 pixel running average

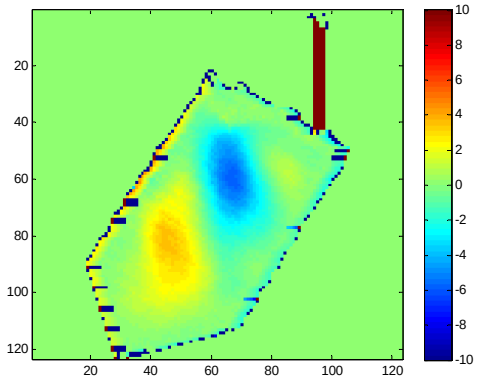

(j) Cross-sun slope; 9 pixel running average

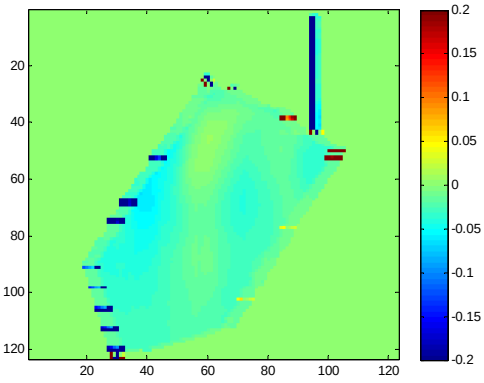

of this DEM, qualitatively, is whether interpolated and original values are distinguishable. Visual inspection and a series of horizontal transects demonstrates that the zones are largely indistinguishable. However, there are notable exceptions where linear deviations are obvious in otherwise smooth topography. These are predominantly the result of the propagation of error from an either saturated or non-snow covered surface; concentrated off of the icecap itself, these blemishes will thus not significantly impact future use of the 2007 DEM.

3.4 Calculation of Glacier Volume Change and Mass Balance

Bringing insight to questions such as global climate change and sea level rise, the mass balance of ice masses ranging in size from small valley glaciers to continental ice sheets presents an interesting and important scientific challenge (Zwally et al. 2002; VanLooy et al. 2006). Traditionally, specific mass balance is an extrapolation based on point snow pit and ablation stake measurements taken on a glacier's surface (e.g. Björnsson et al. 1998; 2002; Miller & Pelto 1999). However, due to significant variability which may not be fully described by the extrapolation method (Björnsson et al. 1998), a synoptic view would be preferable.

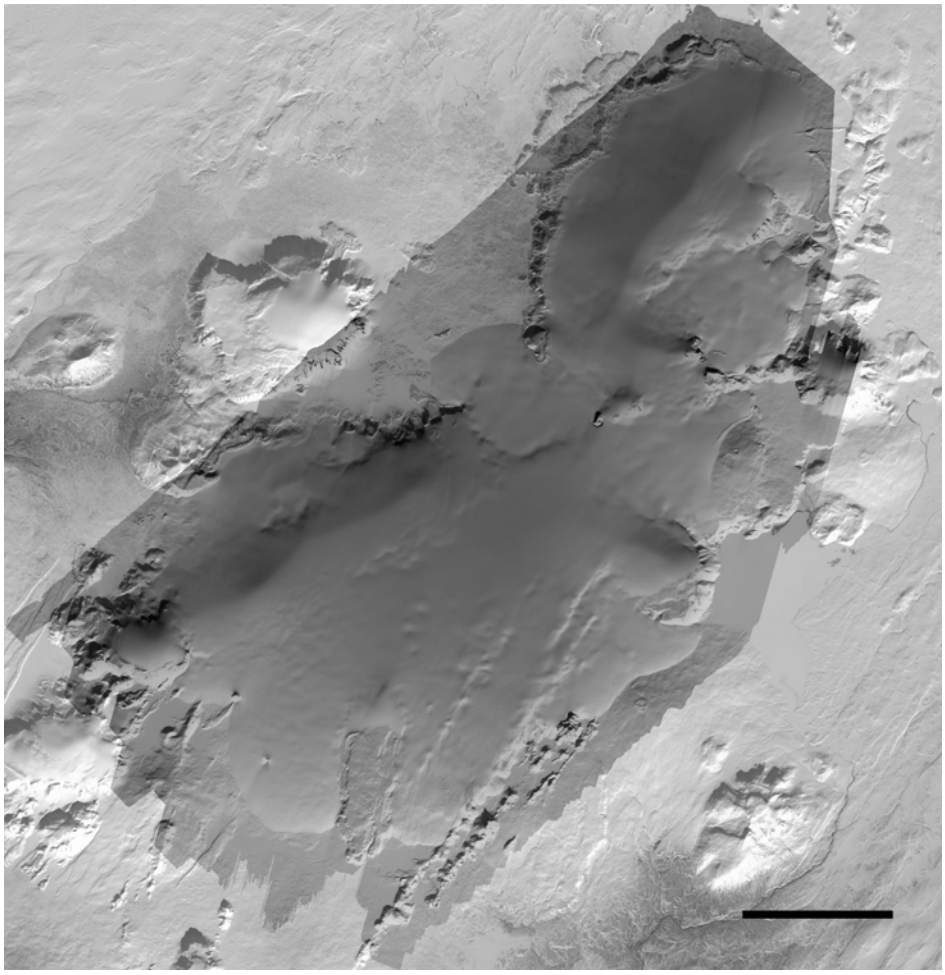

Figure 3.4 *Coverage of final DEM masked over the same image as in Figure 1.8. The scale bar is 10 km.*

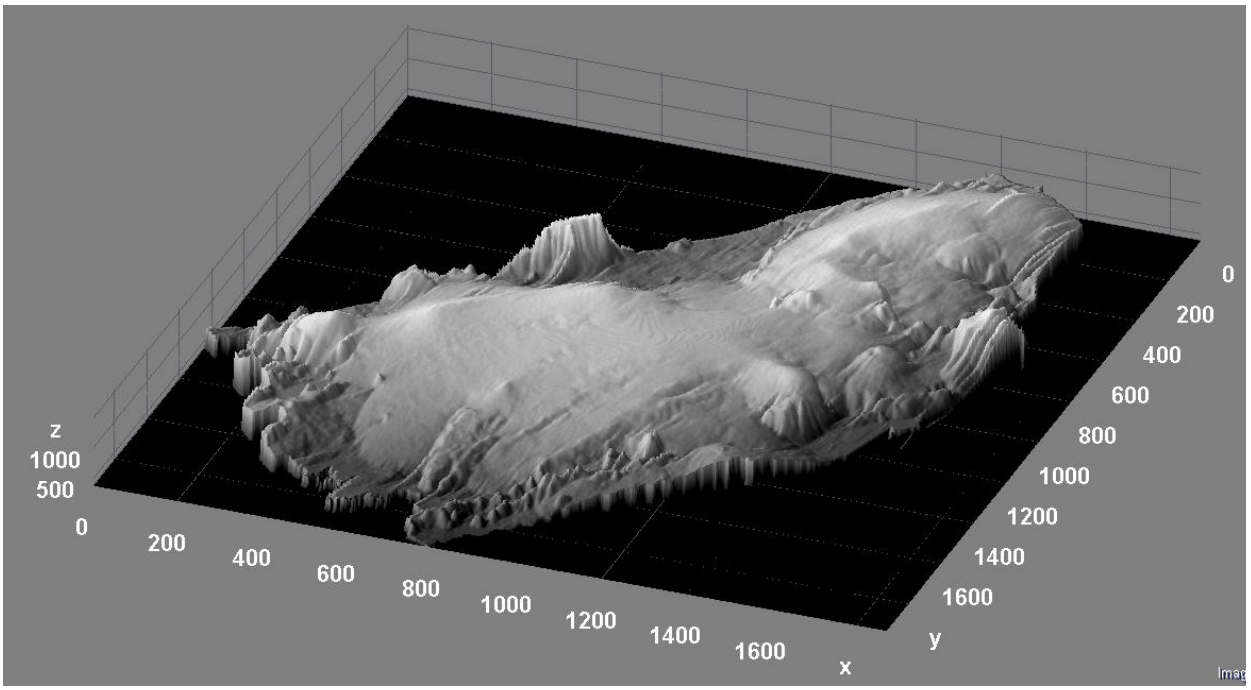

Figure 3.5 *3D visualization of summer 2007 DEM of Langjökull. The x-axis is oriented east-west and the y-axis is aligned north-south; both are measured in 30 m pixels. The z-axis is expressed in meters above sea level. Artificial shading has been added to enhance imaging of the topography.*

Clearly the entire surface of the glacier cannot be excavated, but by comparing DEMs, spatial distribution of elevation change and therefore volume change can be easily calculated across a glacier surface for a given time period. However, volume change does not equate with mass balance. A simple approach relates change in mass (ΔM) to volume change (ΔV) by an approximation of the density (ρ) of the material which has been lost.

$$\Delta M = \rho \, \Delta V \tag{10}$$

Although the assumption of an average density can vary significantly depending on whether glacier ice (0.83-0.91 g cm^{-3}) or young firn ($\geq$ 0.4 g cm^{-3}) has ablated (Patterson 1981), in practice because net ablation generally occurs in bare-ice areas, a density of 0.90 g cm^{-3} allows for glacier ice with air bubbles and some fractures (Miller & Pelto 1999; Rees & Arnold 2007).

In addition, the spatial distribution of volume change is not necessarily indicative of where a glacier has actually lost mass. For example, a surge in flow will result in displacement of material downglacier. In this case, comparison of surface elevations would show accumulation lower in the glacier and ablation upglacier, despite the fact that melting is still impacting the lower regions more than the upper regions. Thus, although the magnitude of volume change would be correct, the spatial distribution component requires further interpretation. By employing a glacial flow model, surface elevation change can be related to location-specific mass balance given additional input parameters such as flow velocity fields or underlying basal topography (e.g. Cogley 1999; Guðmundsson & Bauder 1999; Rasmussen & Krimmel 1999; Hubbard et al. 2000).

Ultimately, the approach taken is dependent on the resources available and the goal of the study. Complex modeling can give insight into the changes in a glacier's flow behavior with relation to spatial distribution of mass balance, but significantly more information and computation is required. Indeed, for monitoring purposes and averaging across a glacier, Equation 10 is more than adequate.

3.4.1 Determining DEM Comparison Error

When using DEMs to calculate elevation and/or volume change, both method-induced error (e.g. the capacity of LiDAR or differential GPS to reproduce a surface) and imperfect registration of surfaces contribute to the eventual uncertainty. These two sources can be combined in a simple model which describes the interaction of surface topography and sources of error:

$$\sigma = \sqrt{\sigma_0^2 + a^2 m^2} \tag{11}$$

where σ is the uncertainty of a calculated elevation difference, σ_0 is its value over a horizontal surface, *m* is the magnitude of the surface slope expressed as a fraction, and *a* is a constant with the dimension of length which combines registration, gridding, and alignment errors (Rees & Arnold 2007). Using a least squares regression of *m* and σ, values of σ_0 and *a* can be determined; by contrasting this uncertainty (σ_0) with the mean elevation difference between DEMs of locations of constant elevation, the uncertainty and systematic bias inherent in the DEM comparison can thereby be evaluated.

4. Results

As mentioned above, this study aims to quantify information regarding Langjökull's evolution including areal extent, volume change, and mass balance from 1997 to 2007 by utilizing relevant sets of remotely sensed data. However, before final results can be calculated, the comparison and its inherent error must first be considered.

4.1 Comparison of DEMs

Given the data sets available, we must determine the accuracy with which it is possible to calculate elevation and volume change across Langjökull. In order to evaluate this uncertainty for the Langjökull DEMs, only non-ice locations for which a slope *m* (see Equation 11) could be calculated from 2007 LiDAR were evaluated; these areas are assumed to have remained at constant elevation between 1997 and 2007. Only LiDAR-measured areas were considered because interpolation over non-ice surfaces is not representative of the DEM as a whole; non-ice areas were determined from a mask made using a summer 1994 Landsat TM image. In addition to calculating the uncertainty, this process was used to identify the best registration of the 1997 and 2007 data sets, whereby the alignment with lowest a and σ_0 values (see Equation 11) and a high R^2 value is chosen. A regression using 209,560 pairs of m and σ yielded $\sigma_0 = 8.08 \pm 0.28\,\text{m}$ and $a = 27.13 \pm 4.43\,\text{m}$ as the best-fitting values. For comparison, the mean elevation difference between bare-rock areas is 2.8 m; therefore, we find no significant systematic error between the two DEMs. In addition, because LiDAR acquisition on a highly reflective glacier surface is more reliable than on low-albedo rock surfaces, and GPS data collection by snowmobile was likely more comprehensive on the glacier surface than surrounding areas, random errors are likely to be less than 8 m on Langjökull's moderately-sloped surface.

4.2 Langjökull Volume Change and Mass Balance

Figure 4.1 illustrates the distribution of elevation change across Langjökull from 1997 to 2007. The data is masked to include all ice surfaces while excluding as much non-ice area as possible; the outline was derived from 1994 and 2007 Landsat images. It can be seen that the dominant shift across Langjökull is that of elevation loss. In particular, outlet Hagafellsjökull Vestari demonstrates a significant retreat over the last decade; Þrístapajökull, on Langjökull's western margin, also shows a clear retreat. Central Langjökull, on the other hand, is characterized by moderated elevation loss, with areas towards the interior even showing

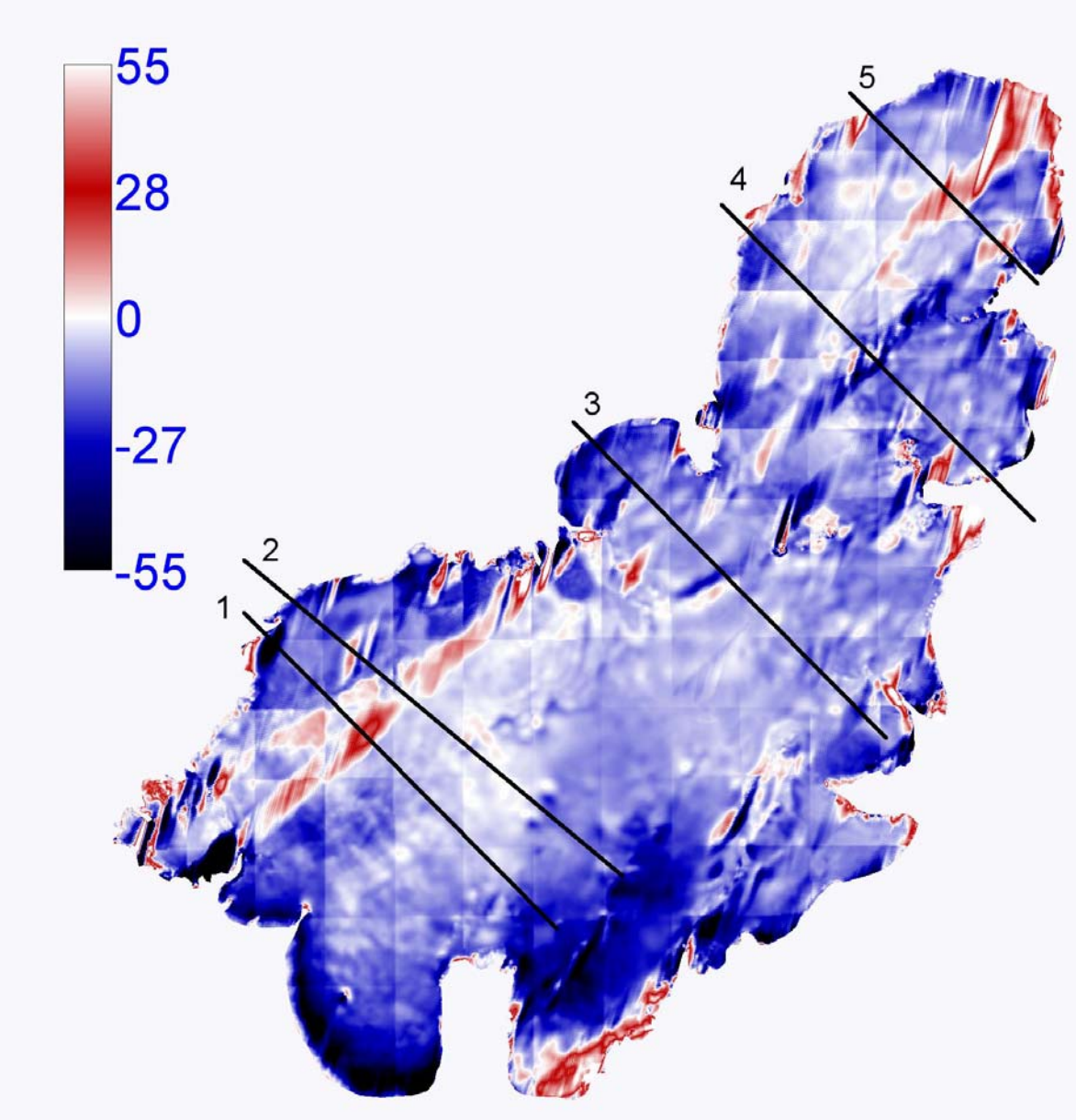

Figure 4.1 *Spatial distribution of elevation change in meters between 1997 and 2007 on Langjökull. Over a measurement period of 10 years, the annualized specific mass balance for Langjökull is -0.99 ± 0.1 m yr^{-1} w.e. Numbered profiles were considered in investigation of systematic error (see Figure 4.2).*

modest elevation gain. Also of note is the increase of elevation at the terminus of outlet Hagafellsjökull Eystri paired with significant elevation loss moving towards its source area. This finding is consistent with a surge of Hagafellsjökull Eystri in 1998, just after the older DEM was produced.

In addition to these observations, there are quite a few observable imperfections in the calculated elevation difference between the 2007 and 1997 DEMs. First are the grid-like artifacts which are the result of a correction to match the Icelandic geoid elevations with the WGS84 ellipsoid; although these discontinuities are known to be well below sub-meter scale, this observation accentuates the importance of understanding the impact of all processing steps in DEM creation. More germane to this study are the readily evident linear

inconsistencies within the DEM at two different scales. Despite a smooth and apparently accurate 2007 DEM, on a large scale there are northeast-southwest oriented areas of both apparent elevation increase and decrease which highlight regions areas where PC interpolation did not work as ideally as hoped. In particular, inconsistencies in the north of Langjökull can be traced to long integration distances imposed by the contribution of 1997 tie points (see Section 3.3.5). On a smaller scale, local discontinuities in elevation change are likely to be the result of saturated or unusually dark pixels interfering with the interpolation process; examples of this are visible on the eastern glacier margins, as well as a noticeable spot in central Langjökull a little east of profile 3 in Figure 4.1.

Moving from the qualitative to the quantitative, the average elevation change across the entire glacier (over one million data points) is calculated to be -11.02 m. Using the ice density approximation (1 m ice ≈ 0.9 m.w.e.) discussed in Section 3.4, this yields a value of -9.92 m.w.e. for Langjökull from 1997 to 2007. Over the measurement period of 10 years, the annual specific mass balance for Langjökull is -0.99 m yr^{-1} w.e. However, recognizing the unknown influence of the errors described above, we must seek to accurately quantify the uncertainty in the values presented here.

4.2.1 Volume Change and Mass Balance Error Assessment

When considering uncertainty in a measurement, one must take into account random error as well as systematic error. While already considered for the process of comparing the two DEMs, the uncertainty inherent in the measurements of ice elevations must still be considered. Random errors from the LiDAR are considered to be ~0.15 m, whereas differential GPS is considered to have a vertical accuracy of ~0.02 m. Nevertheless, even with much larger random uncertainty than this, because of the exceedingly large number of individual points being averaged to calculate total mass change across Langjökull (over one million), the random error is negligible.

Further, systematic error in the PC interpolation process must be carefully considered because it has the potential to significantly influence the calculated values presented above. To investigate the effect of PC interpolation on elevation-difference calculation, 5 transects were taken across Langjökull (for location see Figure 4.1, for results see Figure 4.2). With these transects we hope to identify the scale of systematic error imposed by PC interpolation and the bias which they impart upon eventual elevation difference calculation. Inspection of the profiles yields examples of obvious overestimation (e.g. Profile 1) and underestimation (e.g. Profile 3) as well as areas which blend in very well with surrounding LiDAR-derived

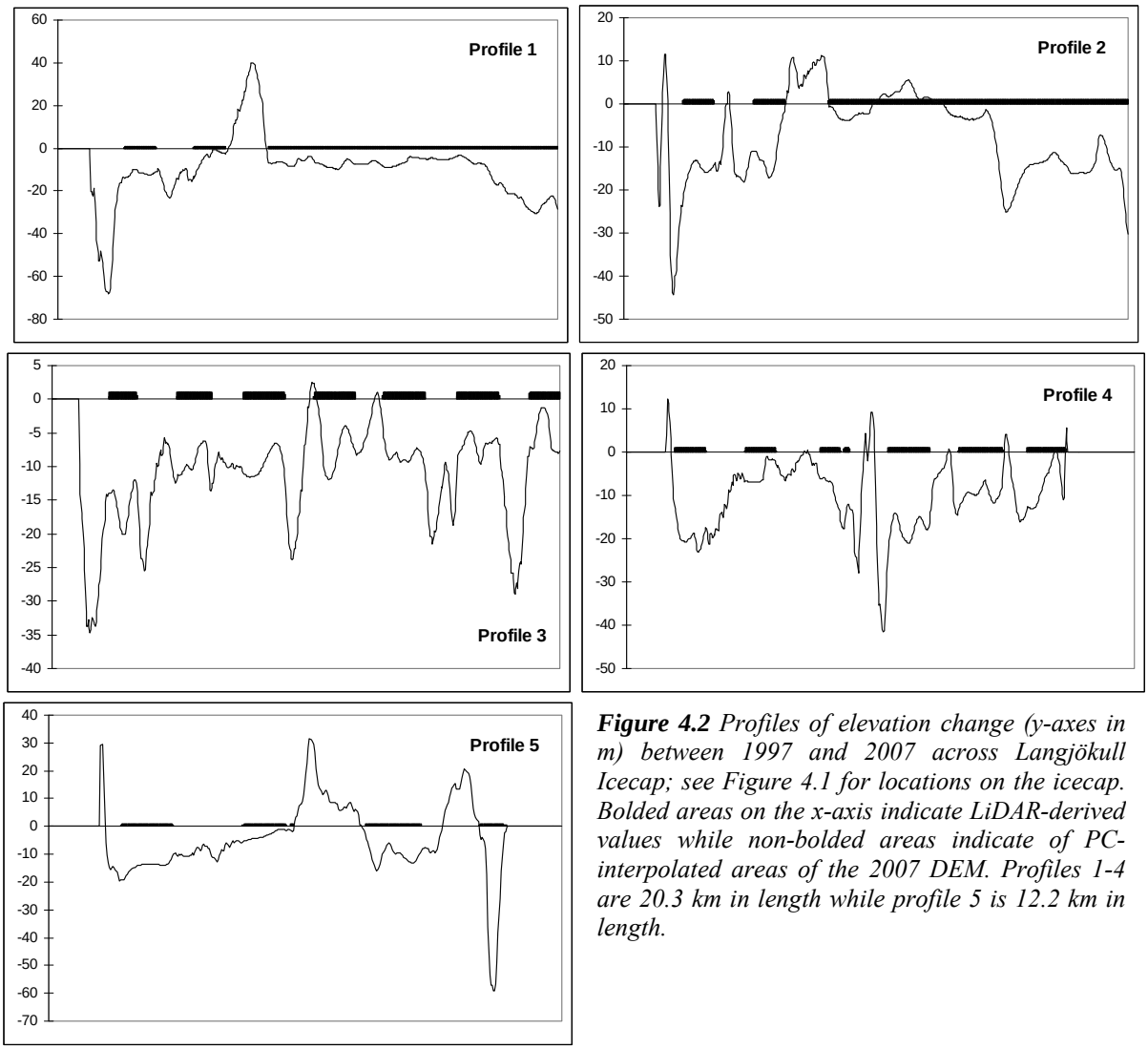

Figure 4.2 *Profiles of elevation change (y-axes in m) between 1997 and 2007 across Langjökull Icecap; see Figure 4.1 for locations on the icecap. Bolded areas on the x-axis indicate LiDAR-derived values while non-bolded areas indicate of PC-interpolated areas of the 2007 DEM. Profiles 1-4 are 20.3 km in length while profile 5 is 12.2 km in length.*

values (e.g. Profiles 4 and 5). However, without further data, it is impossible to definitively identify whether positive or negative deviations exert a dominating influence and the extent to which they do so.

To attempt to provide another point of comparison for PC interpolation-derived elevation change values, a simple model of elevation change across Langjökull is employed. Based on the same mask used in earlier elevation difference calculations, every pixel across Langjökull is assigned a value representing its distance from the edge of the glacier with a Euclidian distance algorithm. In a similar fashion to traditional mass balance measurements which extrapolate point ablation stake and snow pit measurements across the entire glacier based largely on elevation, all LiDAR-derived elevation differences for a given distance from the perimeter are averaged and used to fill in areas of identical edge distance which do not have LiDAR coverage. Figure 4.3 shows that this model does not provide satisfying spatial results for mass balance across Langjökull, as it appears to be continuous with LiDAR-

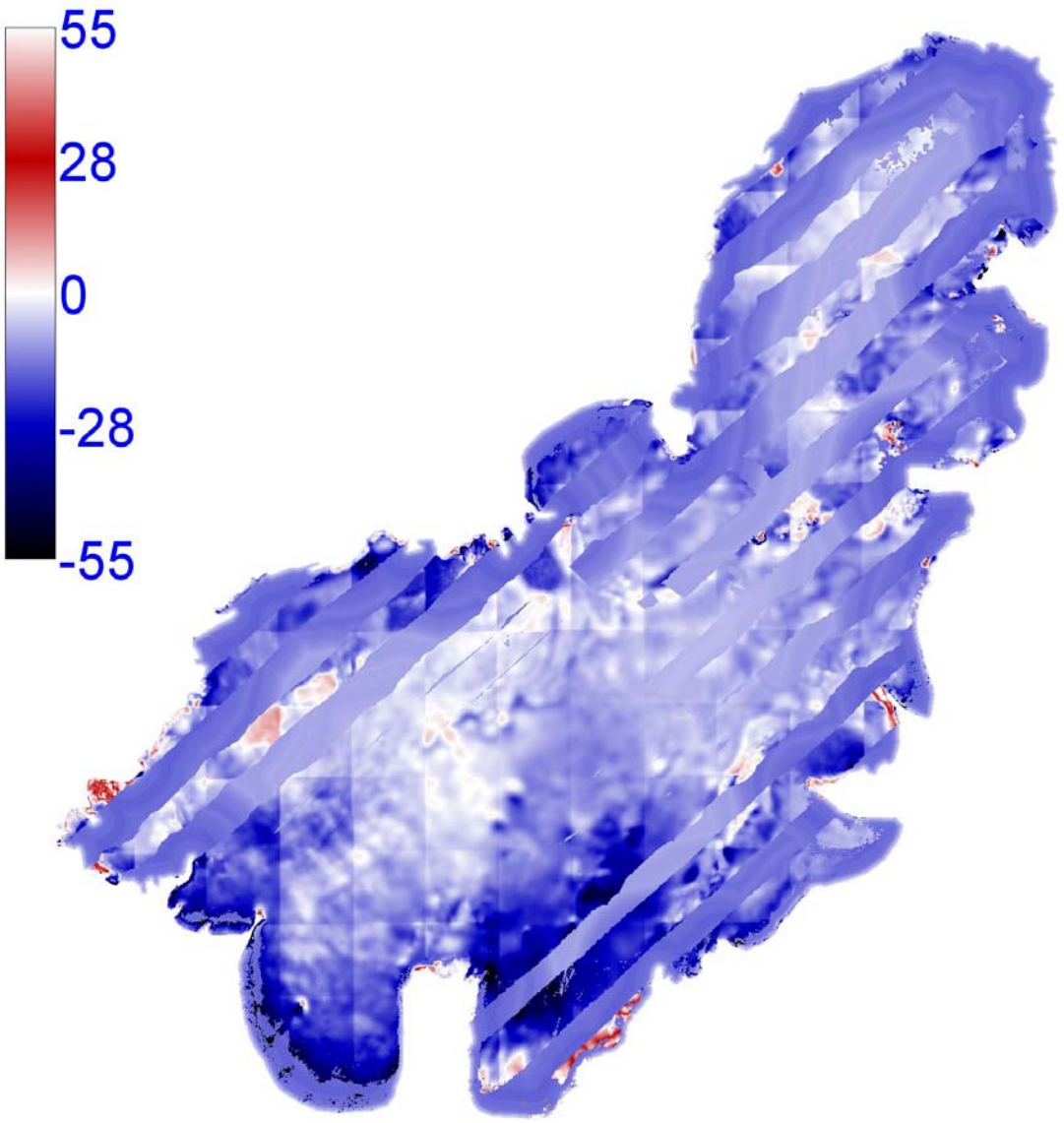

Figure 4.3 *1997 to 2007 elevation change in meters of Langjökull Icecap combining measured values where available and elevation change as a function of distance from glacier perimeter otherwise (see Figure 4.4).*

derived values in only very restricted areas. Indeed, the model is expected to be flawed as it does not include potentially important factors such as glacier aspect and differential precipitation across the icecap resulting from dominant weather patterns. In addition, this model does not reproduce important local observations such as surge indications on Hagafellsjökull Eystri. On the other hand, it is easier to identify likely legitimate local anomalies such as those visible in the southwest of Langjökull in Figure 4.3.

Despite these largely negative observations, this model does emulate a well-reasoned and respected method in order to simply extrapolate LiDAR-derived values across the entirety of Langjökull. It also supplies interesting information regarding Langjökull elevation change, such as the distribution of elevation change as a function of distance from the icecap's

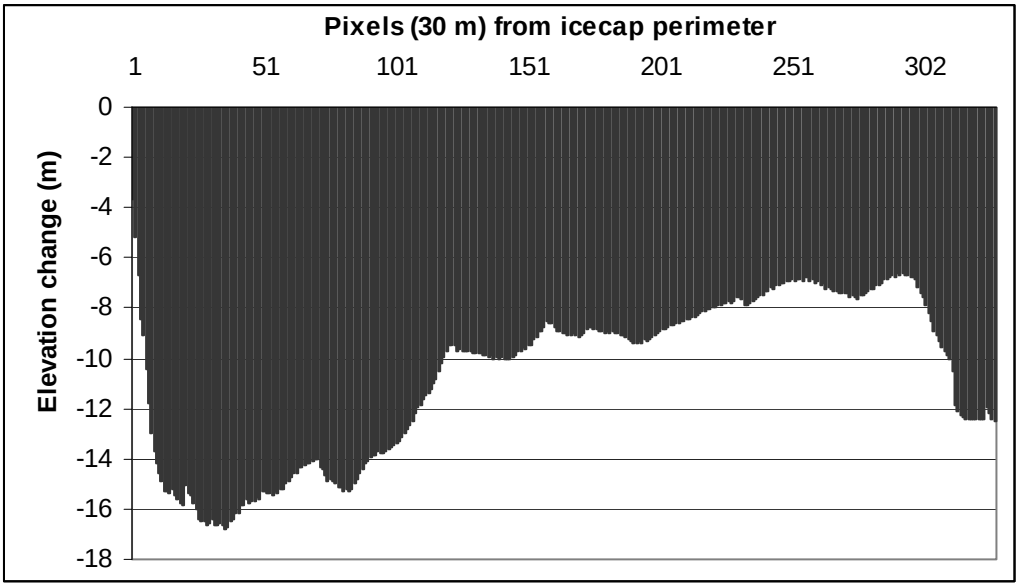

Figure 4.4 *Mean 1997 to 2007 surface elevation change of Langjökull Icecap versus distance from icecap perimeter; distance values were calculated using a mask of glacier extent and a Euclidian distance mapping algorithm.*

perimeter (see Figure 4.4). We see a very strong negative mass balance towards the periphery of Langjökull, recognizing that the first few pixels are likely rock rather than ice. As expected from earlier observations, this negative elevation decreases in magnitude towards the interior of the icecap, except for an unexpected resurgence in negative values for the most interior ice. It is worth noting that while the most interior areas are losing elevation, these are not equivalent to the highest elevation parts of Langjökull, which in fact appear to be gaining elevation (see Figure 4.1).

Although we recognize that these observations are in part a product of where LiDAR data is available, when used to calculated glacier-wide average elevation change, the outcome is -12.14 m or -10.93 m.w.e. Thus, according to this model, the PC-interpolated topography (-9.92 m.w.e.) causes an underrepresentation of elevation decrease across Langjökull. However, we have no reason to believe that the modeled elevation change is necessarily the best either. What we do take away from this exercise is the important knowledge that multiple methods yield very similar results, and that introduction of a 10% uncertainty on PC-interpolated elevation change calculations would lead to strong confidence in reporting an annualized spatially averaged mass balance for Langjökull as -0.99 ± 0.10 m yr^{-1} w.e.

4.3 Areal Change of Langjökull

Information concerning the change in areal extent of Langjökull was determined through manual tracing the icecap's boundaries in end-summer Landsat imagery from 1994, 2001, and 2007. Table 4.1 shows values for Langjökull's total area and change over time; uncertainty is

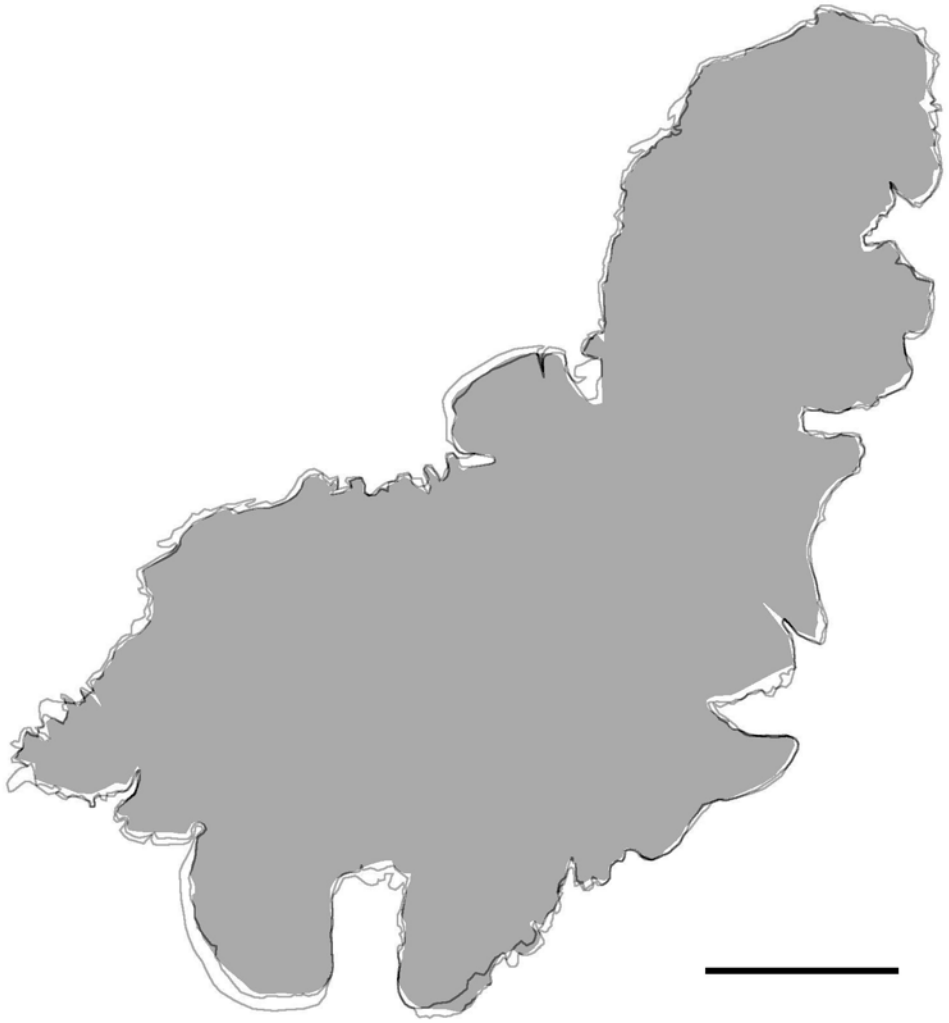

Figure 4.5 *Change of areal extent of Langjökull Icecap from manual tracing of 1994 (trace), 2001 (trace), and 2007 (shaded) Landsat images. The scale bar is 10 km long.*

Table 4.1 *Langjökull areal extent and change over time as determined from Landsat images*

Year(s)	Area or Areal Change (km^2)	Uncertainty (km^2)
1994	942	24.3
2001	916	23.8
2007	898	24.3
1994 to 2001	-26.0	34.1
2001 to 2007	-18.3	34.0
1994 to 2007	-44.3	34.4

determined by identification of the terminus to within ± 3 pixels or 90 m. These values show a definite trend across the last decade of Langjökull shrinking an average of -3.4 ± 2.5 km^2 yr^{-1} from 1994 to 2007. Figure 4.5 shows recession along almost the entire glacier margin, confirming not only the particularly strong recession signal seen from elevation change data on Hagafellsjökull Vestari and to a lesser extent Þrístapajökull, but also visualizing the 1998 surge of Hagafellsjökull Eystri.

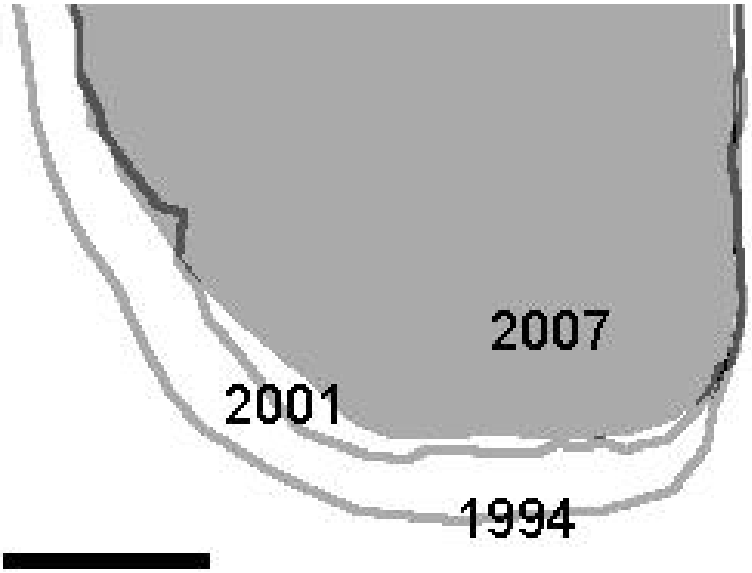

Figure 4.6 *Change of areal extent of Langjökull outlet Hagafellsjökull Vestari from manual tracing of 1994 (trace), 2001 (trace), and 2007 (shaded) Landsat images. The scale bar is 2 km long.*

Table 4.2 *Consideration of registration errors in Hagafellsjökull Vestari DEMs; 5,113 to 10,187 data pairs used.*

Years	σ_0 (m)	*a* (m)	R^2	Mean elevation difference (m)
1997 to 2001	6.34 ± 0.24	271 ± 2490	0.5093	0.75
2001 to 2007	4.49 ± 0.12	18.78 ± 20.74	0.9293	2.60
1997 to 2007	6.05 ± 0.09	36.17 ± 6.63	0.8215	4.40

4.4 Hagafellsjökull Vestari: A Case Study

A closer investigation of Langjökull's largest outlet glacier, Hagafellsjökull Vestari, is facilitated by the addition of a photogrammetrically-derived DEM of the area from 2001 (see Fig 1.8 for outline). Figure 4.6 shows that Hagafellsjökull Vestari receded significantly from 1994 to 2007; although the eastern edge of the glacier is largely pinned to the steep Hagafell Ridge, from 1994 to 2001 the entire terminus retreated, while from 2001 to 2007 only the very snout appears to have withdrawn further.

In terms of volume change, comparison, registration, random, and systematic errors must be considered as they were with regard to measuring elevation across all of Langjökull (see Section 3.4.1). Table 4.2 shows the values of σ_0, *a* (see Equation 11), R^2, and the mean elevation difference on rock surfaces. In all DEM comparisons we see fairly low σ_0 values, which is encouraging, with the lowest value (and highest R^2), as expected, seen between the two highest resolution data sets from 2001 and 2007; most importantly, σ_0 is greater than the mean elevation difference in all cases and we therefore find no pervasive systematic errors between DEMs.

With regard to systematic errors, because PC-interpolation is not a source of significant error in this area of the 2007 DEM, and the residuals have an approximately normal distribution, we consider only random errors. Due to the large number of values contributing to the final result (29,091 data points), random errors become negligible; numerical results are reported in Table 4.3. Figure 4.7 shows the distribution of elevation change across Hagafellsjökull Vestari for the time periods considered here. Like elevation changes for all of Langjökull, the grid artifact can be seen in (a) and (c) where the 1997 DEM is used. Of more consequence, it appears that while most elevation was lost on the terminus from 1997 to 2001, most elevation was lost slightly up-glacier from 2001 to 2007; this agrees with the terminus retreat pattern observed in Figure 4.6. Ultimately, the distribution and magnitude of 1997-2007 elevation change across Hagafellsjökull Vestari show that significant terminus retreat as well as interior melting are shrinking this outlet glacier.

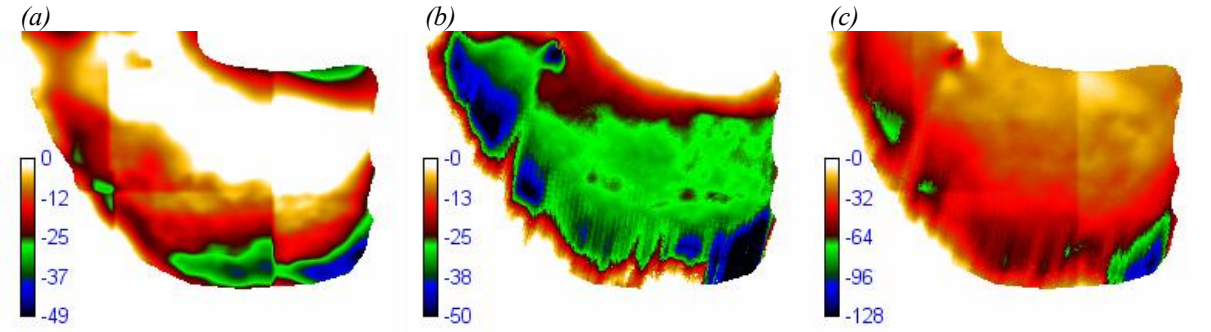

Figure 4.7 *Spatial distribution of elevation change in meters between (a) 1997 to 2001 (b) 2001 to 2007 and (c) 1997 to 2007 on Hagafellsjökull Vestari, Iceland. The annualized spatially averaged mass balances for the outlet during these time periods are -2.28 m yr^{-1} w.e.,-3.86 m yr^{-1} w.e., and -3.23 m yr^{-1} w.e. respectively.*

Table 4.3 *Total and annual elevation differences and mass balances for Hagafellsjökull Vestari terminus*

Year	Type	Elevation Difference (m)	Mass Balance (m.w.e.)
1997-2007	Total	-35.88	-32.39
1997-2001	Total	-10.15	-9.13
2001-2007	Total	-25.73	-23.16
1997-2007	Annual	-3.59	-3.24
1997-2001	Annual	-1.02	-0.91
2001-2007	Annual	-2.57	-2.32

5. Discussion

The results gained through photoclinometric augmentation of an airborne LiDAR-derived data set illustrate and quantify the level to which Langjökull is retreating. Further examination of the method used and contextualization of the quantitative results will allow for crucial evaluation of scientific confidence in the findings and help evaluate mass balance measurement techniques. In addition, it will give insight into how a changing Langjökull may influence the surrounding environment.

5.1 Discussion of Photoclinometry

As with any assessment, the efficacy of a method is predicated upon the task it seeks to complete. Thus, it is difficult to provide a concise yet comprehensive appraisal of DEM creation with photoclinometry (PC) because DEMs have many potential uses. This study addresses the use of DEMs in determining icecap-wide mass balance, and as such, location-specific elevations are not as essential as spatially averaged values. Using PC, a crucial step is the determination of α' and γ' (see Sections 3.1 and 3.3.3); the best practice was decided to be a least squares regression using contiguous data on the most central part of the icecap. However, the sensitivity of final calculations to this decision was previously undetermined. As a test, total mass balance calculations were repeated with α' and γ' varying $\pm 10\%$ from the best-fit values in multiple combinations. Encouragingly, the final result led to a change in final calculated mass balance of less than 3.3%; not only are the values self-consistent, but they vary considerably less than the 10% error adopted in Section 4.2.1.

This small investigation bolsters confidence in the robustness of this application of PC and the results derived thereby. More specifically, the relative consistency of mass balance to changes in PC coefficients means that error in DEM creation should not be seen as a weakness in the method. Instead, more time should be spent considering the quality and appropriateness of the visual imagery used to calculate slope values. Topography of areas with quality imagery can be well represented by PC, whereas inappropriate or lower-quality imagery is likely to be the limiting factor in any application of PC.

Provided confidence in the visual imagery being used as an input, PC can be considered a useful tool for creating DEMs useful for a wide range of tasks. Indeed, a metric of image quality could help quantify the uncertainty in elevations of the eventual DEM. Poor or inappropriate images can result from a wide variety of causes, for example inability of the imager to handle low-contrast regions (Raup et al. 2005), a significant density of high-slope

areas in the image, or an image which is captured at a time when the entire glacier surface does not have homogenous reflective qualities. It is important to recognize limitations inherent to a particular region. Because of its temperate nature and significant topography, Langjökull stretches the extent to which PC can be used; for more success and lower uncertainty, PC application should be biased towards colder, flatter ice masses. Nevertheless, through data collection at the appropriate time (early spring) and with the correct sensor (e.g. calibrated aerial digital photography or the 12-bit Advanced Land Imager rather than the 8-bit Landsat ETM+) results of PC could be improved.

When first considered for application to ice mass surfaces, vertical error from photoclinometry was over 50 m (Rees & Dowdeswell 1988). With improvements in imaging techniques, error from PC DEMs has decreased, and significant success has been had investigating features such as ridges (Goodwin & Vaughan 1995), domes (Scambos et al. 1998), and dolines (Bindschadler et al. 2002). Significantly, published literature utilizing PC is almost exclusively restricted to applications in Greenland and Antarctica where surfaces are highly uniform and have very low relief. It is therefore unsurprising to see that while in some areas on Langjökull PC worked quite well, there are quite a few areas where this was not the case (see Figure 4.1); the inherent variability of Langjökull makes it a challenging candidate for PC.

Bingham and Rees (1999) emphasize that although PC provides an acceptable method for DEM creation, other available techniques such as InSAR (see Section 1.3) should be used preferentially. A decade has passed since Bingham and Rees published that opinion, and methods for measuring topography have since progressed significantly, particularly with the advent of airborne LiDAR capable of remotely measuring large regions with vertical uncertainty less than 0.15 m. Therefore, while airborne LiDAR has given PC significantly more accurate tie points for interpolation, the results must also be compared against a higher standard.

Here, photoclinometry has been shown to be an effective and useful tool for DEM augmentation and creation, and confidence can be placed in the robustness of the eventual mass balance results. Nevertheless, the significant spatially variable errors visible in the final DEM produced in this study demonstrate the inconsistency of PC. While PC is satisfactory, it is important to recognize that other methods for completing a DEM, most specifically more LiDAR coverage, would have been strongly preferable to the LiDAR-PC combined DEM. In addition to lower uncertainty, airborne LiDAR also gives quantifiable considerations of its

possible error, whereas uncertainty determinations with PC must be inferred from tests during method investigations.

That is not to say the PC does not have a place in current and future glaciological research; cases such as this highlight the usefulness of PC, allowing for use of incomplete data sets which would otherwise be of significantly lower utility. In areas of otherwise restricted data collection, PC provides a viable alternative, especially if steps are taken to optimize the application of PC, quality of visible imagery obtained, and its integration with the elevation data. PC could also be useful on a smaller scale, combining aerial photography and differential GPS or ground-based LiDAR to create DEMs of small areas of low relief polar ice while steering clear of overly steep or optically variable areas. On a larger scale, while most satellite altimeters are characterized by very low vertical uncertainties (<15 cm), their exceedingly low density of data points (172 m along-track spacing for ICESat; Zwally et al. 2002) makes them ill-suited for integration with PC techniques. Ultimately, while not recommended as a primary tactic, PC is a useful method to have available in any remote sensing toolbox for obtaining valuable results in an otherwise daunting situation.

5.2 Discussion of Mass Balance

This study focuses on the application of various remote sensing techniques to monitor Langjökull, but additional *in situ* mass balance measurements are also available (see Section 2.3). While comparison of DEMs from 1997 and 2007 yielded an annualized specific mass balance of -0.99 ± 0.10 m yr^{-1} w.e., *in situ* measurements report -1.29 ± 0.19 m yr^{-1} w.e. for the same period (see Figure 5.1). These measurements are very close to but not quite within each others' admittedly somewhat arbitrary uncertainty brackets. The disagreement between these values averaged over a ten year period suggests a systematic disparity between *in situ* and remotely sensed mass balance measurements on Langjökull.

Concerning the DEM comparison-based mass balance conducted by this study, there are a few possible sources of error to consider. The most obvious is the quality of the DEMs involved, but this is already taken into account in uncertainty brackets. PC interpolation in the 2007 DEM could be implicated, but the fact the model based on distance from glacier edge gave an annualized specific mass balance of -1.09 m.w.e. again suggests that interpolation is not a source of bias beyond the uncertainty already expressed. The density assumption of ablated material (see Section 3.4) may be questioned, although in order to rectify the two values, an even higher density material would be needed. The value used (0.9 g cm^{-3}) is just on the edge of glacier ice densities (Patterson 1981), and logically makes sense as most of the

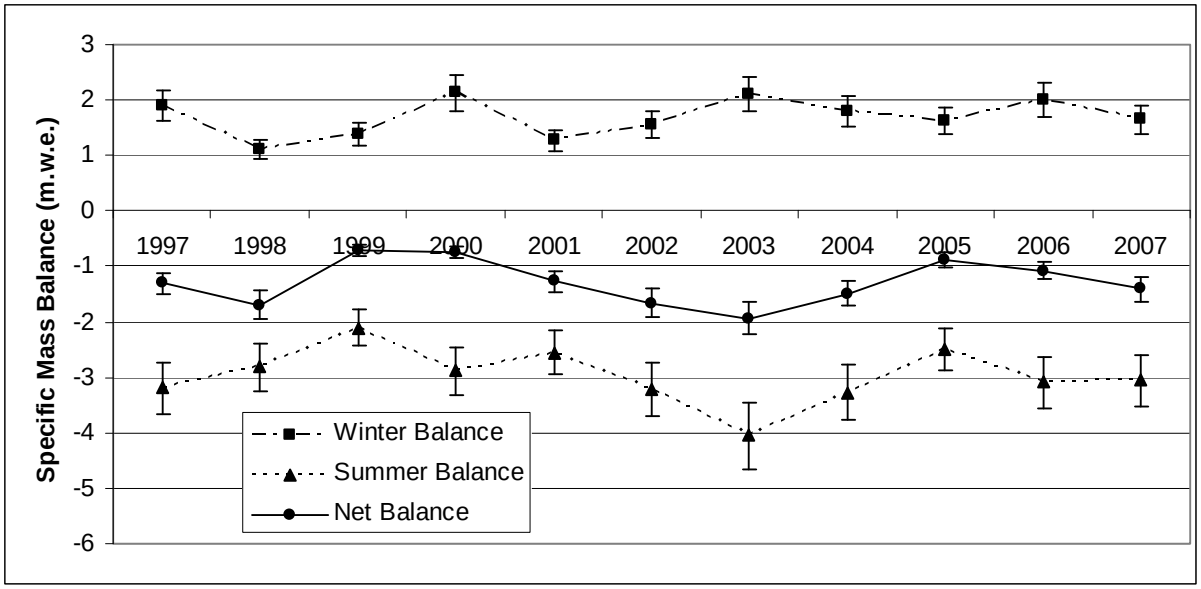

Figure 5.1 *Summer, winter, and net specific mass balance for Langjökull (Pálsson and Björnsson, unpublished data). Error bars are 15%. See Section 2.3 for information on data collection.*

ablated material was likely glacier ice and a little bit of less dense material; even the slight increase to the maximum 0.91 g cm^{-3} cannot explain the offset between specific annualized mass balances. It is possible that some added mass of lower density at higher elevations could have skewed the average mass of volume change. However, this is unlikely because Langjökull's winter balance did not increase over the study period (see Figure 5.1) and there is no reason to believe there has been any recent shift in the rate of firnification on Langjökull. Thus, we instead turn to the *in situ* measurements to explain the inconsistency between mass balance values.

Past studies have also considered occasions where *in situ* mass balance measurements did not match with values calculated from remotely sensed data. For example, Rees and Arnold (2007) observe a significantly more negative mass balance by comparing airborne LiDAR-derived DEMs than that calculated from *in situ* values on Midre Lovénbreen, Svalbard. Although it is possible differing weather conditions may explain this discrepancy, they also suggest that either there is not enough spatial variability in the stake network to describe mass balance as a function of elevation or that the current method of extrapolation does not sufficiently describe the distribution of mass balances across the glacier. Similarly, Rippin et al. (2003) identify remotely sensed mass balances on two glaciers in Svalbard which are significantly more negative than *in situ*-derived values. Again, it is hypothesized that extrapolation techniques may not be sufficient to describe mass balance variability, not only at different elevations, but also due to the different accumulation and ablation characteristics of glacier margins versus central flow lines. Thus, there is agreement within the literature that

current *in situ* mass balance values are unable to account for significant spatial variability either through measurement techniques or extrapolation strategies.

Immediately, an apparent contradiction presents itself; while past studies report *in situ* values less negative than remotely sensed values, here we find that the remotely sensed specific mass balance of Langjökull is less negative than that measured *in situ*. However, it is crucial to recognize that while previous studies consider only a single glacier, here we present comparison of specific mass balance across an entire icecap, with many diverse outlets. Multiple stake profiles are combined in order to theoretically account for mass balance variations based not just on elevation but also lateral differences such as accumulation gradients due to predominant weather patterns. Nevertheless, *in situ* values are still too negative compared to remotely sensed values, suggesting that there is a systematic error with the method of extrapolation being used on Langjökull.

Accumulation and ablation measurements are taken in the center of flowlines, but the morphology of Langjökull, or any icecap, is such that these locations may not necessarily be representative of other large sections of the icecap. It is possible that through focusing on outlet glaciers, the large negative mass balance of Hagafellsjökull Vestari has skewed the mass specific mass balance for all of Langjökull. Indeed, surges in outlet glaciers are also likely to bias extrapolated mass balance values, and the 1998 surge of Hagafellsjökull Eystri must be very difficult to account for with *in situ* measurements. By constructing a stake network along outlet glaciers to correct for elevation and aspect, variation in the diverse, higher accumulation areas may be insufficiently constrained. This is presented as one potential reason for the inconsistency in mass balance reported through *in situ* and remote methods, and it indicates that further consideration of the spatial distribution of mass balance stake measurements on Langjökull and extrapolation techniques for icecap monitoring would be very valuable.

5.2.1 Langjökull's Future

The influence of strong retreat and a significant surge event on Hagafellsjökull Vestari and Eystri, respectively, are the most visible features in the elevation difference map of Langjökull between 1997 and 2007 (see Figure 4.1). These tell about Langjökull's recent behavior, while other details can perhaps shed light on how Langjökull may behave in the future. As it stands now, Langjökull must experience increased winter precipitation and/or decreased temperature to arrest a continued decline (Rasmussen 2005; Flowers et al. 2007). However, if current

reports of melt and climate change are any indication, neither criterion will be Langjökull's fate.

Various past studies have reported the likely timing of Langjökull's demise. Based solely on ablation rate, Björnsson et al. (2005) report complete melt within 200 to 300 years, while a more complex study involving consideration of local topography predicts Langjökull's disappearance around the year 2140 (Björnsson & Pálsson 2008). Assuming a continuation of melt rate determined from 1997 and 2007 DEM comparisons, Langjökull will completely melt by the year 2200 ± 20, although this does not take into account any possible effects of change in glacier elevation distribution or flow behavior. Nevertheless, it confirms very closely the expected future of Langjökull expressed in published literature.

In addition, the distribution of elevation changes across Langjökull may give a subtle clue as to the future behavior of Hagafellsjökull Vestari. It appears that areas in the high accumulation area of Langjökull's largest outlet glacier are increasing in elevation rather than decreasing in correspondence with the rest of the icecap (see Figure 4.1). Similar behavior has been observed in Arctic icecaps (Colgan et al. 2008) and the interior of the Greenland Ice Sheet (e.g. Johannessen et al. 2005). While thickening in Greenland is attributed to increased precipitation resulting from a warmer climate (Zwally et al. 2005), Devon Icecap's elevation increase, coincident with continued negative mass balance as well, is the result of a stiffening in the flow of basal ice thought to be related to penetration of Neogene cooling (Colgan et al. 2008).

Iceland is significantly more temperate than either Greenland or the Canadian Arctic, and recent winter mass balance measurements show no systematic change in precipitation over the past decade (see Figure 5.1). Other studies have implicated temporal variations in firn compaction concerning elevation anomalies, but these are seen to be on the error of centimeters, a tiny fraction of the elevation difference observed on Langjökull (Arthern & Wingham 1998). Instead, it appears that outward flux via ice flow is not keeping pace with inward flux via accumulation, and may be starting the formation of a surface bulge indicative of a surge event (e.g. Björnsson et al. 2003). If this is indeed the case, because interior behavior takes approximately a decade to translate into change in terminal behavior for Icelandic icecaps such as Langjökull (Sigurðsson & Jónsson 1995), Hagafellsjökull Vestari may experience a surge event within the next ten years. This study therefore emphasizes the need for continued observation of Langjökull's topography and mass balance to better understand its proximal and distant future behavior.

5.2.2 Global and Local Impact

As an integral part of the west-central Icelandic landscape, Langjökull is in constant feedback with its surroundings. Unsurprisingly, it has been shown that Langjökull behaves quite similarly to its larger cousin Vatnajökull, although is more susceptible to annual variability in weather patterns due to its smaller size (Björnsson et al. 2002). Similarly, published mass balance values (Sigurðsson 2005) demonstrate that Hofsjökull, a medium-sized icecap located between Vatnajökull and Langjökull (see Figure 1.1), exhibits almost identical mass balance behavior to its neighbors. Therefore, although it is acknowledged that every glacier or icecap is unique and forced by the independent characteristics of its immediate environment, it is expected that conclusions drawn here concerning the regional and global impacts of Langjökull can be somewhat extrapolated to other Icelandic icecaps such as Hofsjökull and Vatnajökull.

Not only do changes in central Iceland influence other glaciers as they influence Langjökull, but Langjökull is a strong force on its surroundings. Regionally, the runoff from Langjökull is critically important as a source of hydropower and downstream water consumption. The melt rate from 1997 to 2007 suggests that Langjökull will continue to be a strong source of water for the watersheds it contributes to until it is depleted, as has been suggested will occur in ~200 years. More globally, through its melt Langjökull will continue to contribute to global sea level rise. Assuming no acceleration of melt rate, by 2100 icecaps and glaciers around the world will contribute 104 ± 25 mm to global sea level, the Greenland Ice Sheet will contribute 47 ± 8 mm, the West Antarctic Ice Sheet will contribute 20 ± 4 mm, the East Antarctic Ice Sheet will contribute 15 ± 7 mm (Meier et al. 2007), and Langjökull by itself will contribute 0.25 mm. Although not an empirically large sea level rise, 0.25 mm from a small North Atlantic icecap such as Langjökull illustrates the extent to which small ice masses contribute significant amounts of water to the world's oceans.

In addition to the influence that runoff has on it's surroundings, the very disappearance of mass from an icecap can also strongly influence the immediate area; GPS survey studies have shown that due to mass loss from Vatnajökull, the surrounding land is undergoing uplift on the order of 5-10 mm yr^{-1} (Sjöberg et al. 2004). Although Langjökull is smaller than Vatnajökull, it is nevertheless expected that the significant amount of mass loss from Langjökull should cause a similar response, possibly visible in changing features of proglacial lakes. Even further, geodetic studies which quantify land uplift near Langjökull could investigate hetero- or homogeneity in the character of the asthenosphere and lithosphere in

central Iceland, an area of considerable interest considering its position astride a spreading ridge.

5.3 Discussion of Areal Change and Marginal Retreat

While indicative of Langjökull's shrinking size, uncertainties in areal change calculations from 1994-2001 and 2001-2007 allow for either expansion or recession. However, consideration of the entire range from 1994 to 2007 provides definite evidence that Langjökull is shrinking, and at a rate of -3.4 ± 2.5 km^2 yr^{-1}. The diminishing areal extent of Langjökull corresponds well with strongly negative mass balance as measured both by traditional and remote sensing methods.

In particular, Langjökull outlets with a southern aspect are receding the fastest out of any of the icecap's glaciers. This trend towards southern melting is similar to modeled and empirical findings on other Icelandic icecaps (De Ruyter De Wildt et al. 2003; Aðalgeirsdóttir et al. 2006). Simple surface energy balance considerations explain this trend; in summer, solar radiation contributes to melt of the glacier surface and decreases the albedo, thereby initiating a positive feedback loop, especially when the snowpack is depleted and the surface remaining is relatively dark glacier ice. While some High Arctic glaciers influenced by 24-hour summer at a near-constant solar zenith angle sunlight see strongest retreat on northern-aspect outlets (Arnold et al. 2006b), Langjökull's sub-Arctic position means that high-angle, powerful solar radiation influences southern aspect glaciers significantly more than lower angle incident radiation from any other direction.

While published data on monitoring the complete extent of Langjökull is unavailable, frequent reports on the state of Icelandic glaciers do provide information on the fluctuation of icecap outlet glacier termini. Germane to this study are reports on Langjökull outlets Hagafellsjökull Vestari, Hagafellsjökull Eystri, Jökulkrókur, and Kirkjujökull (see Figure 1.6; Sigurðsson 2000; 2002; 2003; 2004; 2005; 2006). Again, the 1998 surge of Hagafellsjökull Eystri was identified, although the uneven terminus makes it a non-ideal candidate for terminus monitoring. While Jökulkrókur and Kirkjujökull underwent retreat, the magnitude of this change is on the edge of Landsat resolution sensitivity. Hagafellsjökull Vestari, on the other hand, was characterized over the past decade by a strong and easily observable retreat (see Figures 4.5 and 4.6).

While elevation data, in particular PC-interpolated area, are not well suited to glacier terminus detection, visible imagery such as Landsat has been referenced as the preferred method for glacier terminus monitoring (Rees & Arnold 2007). As measured by Landsat,

Hagafellsjökull Vestari retreated an average of 86 ± 9 m yr^{-1} from 1994 to 2001, and 35 ± 10 m yr^{-1} from 2001 to 2007. By comparison, Sigurðsson (2000; 2002; 2003; 2004; 2005; 2006) reports an average retreat of 62 m yr^{-1} for 1994 to 2001 and does not have data for more recent changes. The 1994-2001 values are in the same order of magnitude, reinforcing the impression of a strong retreat of Hagafellsjökull Vestari. However, without more recent field data and more specific knowledge of the methods employed *in situ*, further comparisons or conclusions are hampered.

It is interesting to note that according to 1997, 2001, and 2007 DEMs and Landsat extent measurement, the less negative mass balance of the outlet Hagafellsjökull Vestari between 1997 and 2001 (-2.28 m yr^{-1} w.e.) corresponds with a powerful terminal retreat while the more negative mass balance from 2001-2007 (-3.86 m yr^{-1} w.e.) is paired with a more moderate terminal retreat and an increase in mass loss slightly upglacier from the terminus. While it is possible that this shift is part of a continued response to the 1980 surge of Hagafellsjökull Vestari, whereby the glacier was overextended, such a response time would be anomalously long, especially considering the already-retreating Hagafellsjökull Eystri after its considerably more recent surge event. Alternately, some other mass flux-related anomaly may be linked to the change in terminal behavior, but such a change is not readily noticed on other outlets of Langjökull. As such, it is possible that the rapid terminus retreat and subsequently more negative mass balance are additional signs of a possible future surge of Hagafellsjökull Vestari. Or, perhaps the basal topography underlying Hagafellsjökull Vestari has allowed the glacier to attain a more stable terminus location, whereby it is expected that one would see increased melting slightly further upglacier. Further flow modeling would be required to prove or refute these theories. Whatever the reason, it is readily evident that the perimeter of Hagafellsjökull Vestari has stayed fairly constant where it is adjacent to the Hagafell Ridge while strongly retreating on its wider lobe and that such a trend of retreat is likely to continue in the long run.

6. Conclusion

Airborne LiDAR has been shown to be a highly effective technique for measuring glacial topography and building DEMs of ice surfaces. Using the technique of photoclinometry, this study successfully augmented an incomplete airborne LiDAR survey of Langjökull, Iceland with freely available Landsat ETM+ imagery to build a complete picture of the icecap's surface in summer 2007.

In the past, photoclinometry (PC) has successfully been used to interpolate ice surfaces between known tie points and enhance the resolution of large DEMs; for the first time, this study integrated PC with very high resolution spatial data of a glacier surface. Best practice for the data sets involved was determined, in particular selection of Landsat ETM+ band 4 as the best representation of ice surface topography, application of integration and linear scaling between known tie points, and local smoothing by a five pixel running average to remove PC artifacts. We find that PC proves to be a robust technique for topographic reconstruction (RMS error = 3.4 m over a 3 km section). In fulfillment of a primary aim of this study, the photoclinometric technique developed here was able to provide a satisfactory and fully completed DEM of Langjökull useable for further glaciological investigations.

The 2007 Langjökull DEM was evaluated, and although largely faithful to the true surface, there were some inconsistencies. Accuracy in future applications of PC can be ensured by restricting reconstruction to an area which does not have a slope that is too high. Even more importantly, it is crucial that the visible imagery being used for interpolation is of the highest quality, in particular focusing on the consistent ability of the imager to accurately represent low contrast surfaces. In addition, consideration of setting characteristics such as solar azimuth can make later interpolation with PC more effective. While airborne LiDAR remains the preferred method for terrain measurement, PC should be held as a valuable technique when direct measurement is no longer an option and interpolation is necessary.

With the data set produced from LiDAR and PC, the glaciological study proceeded as originally planned. In addition to clear visualization of a retreat of outlet Hagafellsjökull Vestari and the aftereffects of a 1998 surge of Hagafellsjökull Eystri, a simple density assumption was used to determine that between 1997 and 2007, Langjökull had an specific annual mass balance of -0.99 ± 0.1 m yr^{-1} w.e. Consideration of solely the terminus of Hagafellsjökull Vestari using DEMs from 1997, 2001, and 2007 allowed for calculation of the significantly larger annualized spatially averaged mass balances of -2.28 m yr^{-1} w.e. for 1997-2001, -3.86 m yr^{-1} w.e. for 2001-2007, and -3.23 m yr^{-1} w.e. for 1997-2007. To complement these mass balance measurements, manual tracing of Landsat imagery was used to measure

Langjökull's areal extent; satellite images show a definite trend of recession, averaging -3.4 ± 2.5 km^2 yr^{-1} from 1994 to 2007. In sum, remotely sensed elevation change, mass balance and areal change were able to give a clear picture of Langjökull's behavior in the recent past.

These observations, indicating a continued shrinkage of Langjökull, are consistent with published works predicting the disappearance of the icecap, Iceland's second largest, in approximately 200 years. This major mass loss is likely to have many effects including local glacio-isostatic uplift, a continued contribution to global sea level rise, and a dramatic shift in the supply of major watersheds in central and western Iceland. More proximally, slight elevation increases in interior Langjökull paired with anti-correlated terminal retreat and negative mass balance of Hagafellsjökull Vestari could indicate a potential surge of the outlet sometime within the next decade, an event which last took place in 1980 and 1971.

In addressing another aim of this study, comparison of DEM-derived data and *in situ* mass balance measurements revealed a possible systematic difference in the values over the 1997-2007 time period. While past studies on small mountain glaciers have reported that *in situ* measurements yield a more positive specific mass balance than DEM comparison, here we find that *in situ* measurements give a more negative specific mass balance than remote sensing methods; this suggests the possibility that the signal from strongly receding outlets such as Hagafellsjökull Vestari may be skewing the mass balance value calculated for the entire icecap. Careful consideration should be given to how *in situ* measurements are extrapolated to entire icecaps, how this differs from methods used in single glacier systems, how the protocol can be improved with the data that remote sensing techniques are able to provide, and what any systematic shift may mean for *in situ* mass balance studies on other icecaps.

Ultimately, this study is extremely successful in both its technological and glaciological aims by providing both suggestions for future application of PC as well as a much needed benchmark for Langjökull. Photoclinometry is proven to be a current and valuable technique while confirming its status as a secondary rather than primary tool. In addition, glaciological observations recommend continued observation efforts on Langjökull, especially with respect to ongoing mass balance and a potential surge event, and the DEM and mass balance data presented here provide future research opportunities in many disciplines. Studies incorporating the results and techniques laid out by this study will not only help elucidate local hydrology, environmental change, and tectonic properties, but yield a better understanding of the very way that icecap mass balance is calculated for glacial monitoring in general.

7. References

Aðalgeirsdóttir, G., Echelmeyer, K. & Harrison, W.D., 1998. Elevation and volume changes on the Harding Icefield, Alaska. *Journal of Glaciology*, 44(148), 570-582.

Aðalgeirsdóttir, G., Gudmundsson, G.H. & Björnsson, H., 2005. Volume sensitivity of Vatnajökull Ice Cap, Iceland, to perturbations in equilibrium line altitude. *Journal of Geophysical Research*, 110, F04001.

Aðalgeirsdóttir, G. et al., 2006. Response of Hofsjökull and southern Vatnajökull, Iceland, to climate change. *Journal of Geophysical Research*, 111, F03001.

Anderson, J.B., 1999. *Antarctic Marine Geology*, New York: Cambridge University Press.

Andrews, J.T., 2008. The role of the Iceland Ice Sheet in the North Atlantic during the late Quaternary: a review and evidence from Denmark Strait. *Journal of Quaternary Science*, 23(1), 3-20.

Anschutz, H. et al., 2007. Investigating small-scale variations of the recent accumulation rate in coastal Dronning Maud Land, East Antarctica. *Annals of Glaciology*, 26, 14-21.

Anschutz, H. et al., 2008. Small-scale spatio-temporal characteristics of accumulation rates in western Dronning Maud Land, Antarctica. *Journal of Glaciology*, 54(185), 315-323.

Arnold, N.S., Rees, W.G., Devereux, B.J. et al., 2006a. Evaluating the potential of high-resolution airborne LiDAR data in glaciology. *International Journal of Remote Sensing*, 27(5-6), 1233-1251.

Arnold, N.S., Rees, W.G., Hodson, A.J. et al., 2006b. Topographic controls on the surface energy balance of a high Arctic valley glacier. *Journal of Geophysical Research*, 111, F02011.

Arthern, R.J. & Wingham, D.J., 1998. The Natural Fluctuations of Firn Densification and Their Effect on the Geodetic Determination of Ice Sheet Mass Balance. *Climatic Change*, 40(3), 605-624.

Bamber, J.L. et al., 2005. Elevation changes measured on Svalbard glaciers and ice caps from airborne laser data. *Annals of Glaciology*, 42, 202-208.

Barrand, N.E. et al., 2009. Optimizing photogrammetric DEMs for glacier volume change assessment using laser-scanning derived ground-control point. *Journal of Glaciology*, 55(189), 106-116.

Bennett, M.R., Huddart, D. & Waller, R.I., 2005. The interaction of a surging glacier with a seasonally frozen foreland: Hagafellsjokull-Eystri, Iceland. In *Cryospheric Systems: Glaciers and Permafrost*. Geological Society Special Publication. London: The Geological Society, pp. 51-62.

Bennett, M.R., Huddart, D. & McCormick, T., 2000. An integrated approach to the study of glaciolacustrine landforms and sediments: a case study from Hagavatn, Iceland. *Quaternary Science Reviews*, 19(7), 633-665.

Berthier, E. et al., 2006. Biases of SRTM in high-mountain areas: Implications for the monitoring of glacier volume changes. *Geophysical Research Letters*, 33, L08502.

Bindschadler, R. et al., 2002. Ice dolines on Larsen Ice Shelf, Antarctica. *Annals of Glaciology*, 34, 283-290.

Bindschadler, R. & Vornberger, P., 1994. Detailed elevation map of Ice Stream C, Antarctica, using satellite imagery and airborne radar. *Annals of Glaciology*, 20, 327-335.

Bingham, A.W. & Rees, W.G., 1999. Construction of a high-resolution DEM of an Arctic ice cap using shape-from-shading . *International Journal of Remote Sensing*, 20(15-16), 3231-3242.

Björnsson, H., 2002. Subglacial lakes and jökulhlaups in Iceland. *Global and Planetary Change*, 35(3-4), 255-271.

Björnsson, H. & Pálsson, F., 2008. Icelandic Glaciers. *Jökull* , 58, 365-386.

Björnsson, H. et al., 2005. Mass balance of Vatnajökull (1991-2004) and Langjökull (1996-2004) ice caps, Iceland. In *European Geophysical Union Meeting*.

Björnsson, H. et al., 1998. Mass balance of western and northern Vatnajökull, Iceland, 1991-1995. *Jökull* , 45, 35-38.

Björnsson, H., Pálsson, F. & Haraldsson, H.H., 2002. Mass Balance of Vatnajökull (1991-2001) and Langjökull (1996-2001), Iceland. *Jökull* , 51, 75-78.

Björnsson, H. et al., 2003. Surges of glaciers in Iceland. *Annals of Glaciology*, 36, 82-90.

Björnsson, H. et al., 2001. Glacier-volcano interactions deduced by SAR interferometry. *Journal of Glaciology*, 47(156), 58-70.

Boloorani, A.D., Erasmi, S. & Kappas, M., 2008. Multi-source image reconstruction: exploitation of EO-1/ALI in Landsat-7/ETM+ SLC-off gap filling. In *Image Processing: Algorithms and Systems VI*. San Jose, CA, USA: SPIE, pp. 681219-12. Available at: http://link.aip.org/link/?PSI/6812/681219/1 [Accessed February 16, 2009].

Bradwell, T., Dugmore, A.J. & Sugden, D.E., 2006. The Little Ice Age glacier maximum in Iceland and the North Atlantic Oscillation: evidence from Lambatungnajökull, southeast Iceland. *Boreas*, 35(1), 61.

Braithwaite, R.J., 2005. Mass-balance characteristics of arctic glaciers. *Annals of Glaciology*, 42, 225-229.

Brown, I.A., Kirkbride, M.P. & Vaughan, R.A., 1999. Find the firn line! The suitability of ERS-1 and ERS-2 SAR - data for the analysis of glacier facies on Icelandic icecaps. *International Journal of Remote Sensing*, 20(15), 3217.

Cheshire, J., 2008. *Mapping Glacier Surface Change Using Geostatistics: A New Approach on the Juneau Icefield Plateau, British Columbia*. B.A. University of Southampton.

Choudhury, B.J. & Chang, A.T.C., 1981. On the angular variation of solar reflectance of snow. *Journal of Geophysical Research*, 86(C1), 465-472.

Cogley, J.G., 1999. Effective Sample Size for Glacier Mass Balance. *Geografiska Annaler. Series A, Physical Geography*, 81(4), 497-507.

Colgan, W., Davis, J. & Sharp, M., 2008. Is the high-elevation region of Devon Ice Cap thickening? *Journal of Glaciology*, 54, 428-436.

Cooper, A., 1994. A simple shape-from-shading algorithm applied to images of ice-covered terrain. *Geoscience and Remote Sensing, IEEE Transactions on*, 32(6), 1196-1198.

Csathó, B. et al., 2005. ICESat measurements reveal complex pattern of elevation changes on Siple Coast ice streams, Antarctica. *Geophysical Research Letters*, 32, L23S04.

De Ruyter De Wildt, M.S., Oerlemans, J. & Björnsson, H., 2003. A calibrated mass balance model from Vatnajökull, Iceland. *Jökull*, 52, 1-20.

Deems, J.S., Fassnacht, S.R. & Elder, K.J., 2006. Fractal Distribution of Snow Depth from Lidar Data. *Journal of Hydrometeorology*, 7(2), 285-297 .

Deems, J.S., Fassnacht, S.R. & Elder, K.J., 2008. Interannual Consistency in Fractal Snow Depth Patterns at Two Colorado Mountain Sites. *Journal of Hydrometeorology*, 9(5), 977-988 .

Demuth, M. & Pietroniro, A., 1999. Inferring Glacier Mass Balance Using RADARSAT: Results from Peyto Glacier, Canada. *Geografiska Annaler. Series A, Physical Geography*, 81(4), 521-540.

Dowdeswell, J.A., Glazovsky, A.F. & Macheret, Y.Y., 1995. Ice Divides and Drainage Basins on the Ice Caps of Franz Josef Land, Russian High Arctic, Defined from Landsat, KFA-1000, and ERS-1 SAR Satellite Imagery. *Arctic and Alpine Research*, 27(3), 264-270.

Dulova, I. et al., 2008. Reconstruction of the surface topography from single images with the photometric method. *Solar System Research*, 42(6), 522-535.

Echelmeyer, K. et al., 1996. Airborne surface profiling of glaciers: A case-study in Alaska. *Journal of Glaciology*, 42(142), 538-547.

Evans, D.J.A., Lemmen, D.S. & Rea, B.R., 1999. Glacial landsystems of the southwest Laurentide Ice Sheet: modern Icelandic analogues. *Journal of Quaternary Science*, 14(7), 673-691.

Eyre, N.S. et al., 2005. The use of salt injection and conductivity monitoring to infer near-margin hydrological conditions on Vestari-Hagafellsjokull, Iceland. *Annals of Glaciology*, 40, 83-88.

Favey, E. et al., 1999. Evaluating the Potential of an Airborne Laser-Scanning System for Measuring Volume Changes of Glaciers. *Geografiska Annaler. Series A, Physical Geography*, 81(4), 555-561.

Flowers, G.E. et al., 2008. Holocene climate conditions and glacier variation in central Iceland from physical modelling and empirical evidence. *Quaternary Science Reviews*, 27(7-8), 797-813.

Flowers, G.E. et al., 2007. Glacier fluctuation and inferred climatology of Langjökull ice cap through the Little Ice Age. *Quaternary Science Reviews*, 26(19-21), 2337-2353.

Garvin, J. & Williams, R.S., 1993. Geodetic airborne laser altimetry of Breidamerkurjokull and Skeidararjokull, Iceland and Jakobshavns-Isbrae, West Greenland. *Annals of Glaciology*, 17, 379-385.

Geist, T. et al., 2005. Investigations on intra-annual elevation changes using multi-temporal airborne laser scanning data: case study Engabreen, Norway. *Annals of Glaciology*, 42, 195-201.

Gelli, D. & Vitulano, D., 2004. Exploiting light projection for Shape from Shading. *Applied Numerical Mathematics*, 51(4), 535-548.

Goodwin, A. & Vaughan, D.G., 1995. A topographic origin for double-ridge features in visible imagery of ice divides in Antarctica. *Journal of Glaciology*, 41(139), 483-489.

Guðmundsson, G.H. & Bauder, A., 1999. Towards an Indirect Determination of the Mass-Balance Distribution of Glaciers Using the Kinematic Boundary Condition. *Geografiska Annaler. Series A, Physical Geography*, 81(4), 575-583.

Guðmundsson, S., Sigmundsson, F. & Carstensen, J.M., 2002. Three-dimensional surface motion maps estimated from combined interferometric synthetic aperture radar and GPS data. *Journal of Geophysical Research*, 107(B10), 2250.

Haeberli, W. et al., 1999. On Rates and Acceleration Trends of Global Glacier Mass Changes. *Geografiska Annaler. Series A, Physical Geography*, 81(4), 585-591.

Hagen, J.O. et al., 2005. Geometry changes on Svalbard glaciers: mass-balance or dynamic response? *Annals of Glaciology*, 42, 255-261.

Hall, D.K., Riggs, G.A. & Salomonson, V.V., 1995a. Development of methods for mapping global snow cover using moderate resolution imaging spectroradiometer data. *Remote Sensing of Environment*, 54(2), 127-140.

Hall, D.K., Williams, R.S. & Sigurðsson, O., 1995b. Glaciological observations of Bruarjokull, Iceland, using synthetic aperture radar and thematic mapper satellite data. *Annals of Glaciology*, 21, 271-276.

Hanna, E., Jónsson, T. & Box, J.E., 2004. An Analysis of Icelandic Climate Since the Nineteenth Century. *International Journal of Climatology*, 24, 1193-1210.

Howard, A.D., Blasius, K.R. & Cutts, J.A., 1982. Photoclinometric determination of the topography of the Martian north polar cap. *Icarus*, 50(2-3), 245-258.

Holmlund, P. & Jansson, P., 1999. The Tarfala Mass Balance Programme. *Geografiska Annaler. Series A, Physical Geography*, 81(4), 621-631.

Hubbard, A., 2006. The validation and sensitivity of a model of the Icelandic ice sheet. *Quaternary Science Reviews*, 25(17-18), 2297-2313.

Hubbard, A. et al., 2006. A modelling insight into the Icelandic Last Glacial Maximum ice sheet. *Quaternary Science Reviews*, 25(17-18), 2283-2296.

Hubbard, A. et al., 2000. Glacier mass-balance determination by remote sensing and high-resolution modelling. *Journal of Glaciology*, 46(154), 491-498.

Hurrell, J.W., 1995. Decadal Trends in the North Atlantic Oscillation: Regional Temperatures and Precipitation. *Science*, 269(5224), 676-679.

Hurt, N.E., 1991. Mathematical methods in shape-from-shading: a review of recent results. *Acta Applicandae Mathematicae*, 23, 163-188.

IPCC, 2007. Summary for policymakers. In S. Solomon, ed. *Climate change 2007: the physical science basis. Contribution of Working Group I to the Fourth Assessment Report of the Intergovernmental Panel on Climate Change*. Cambridge: Cambridge University Press.

Johannessen, O.M. et al., 2005. Recent Ice-Sheet Growth in the Interior of Greenland. *Science*, 310(5750), 1013-1016.

Jóhannesson, T. & Sigurðsson, O., 1998. Interpretation of glacier variations in Iceland 1930-1995. *Jökull* , 45, 27-33.

Joughin, I. et al., 2009. Basal conditions for Pine Island and Thwaites Glaciers, West Antarctica, determined using satellite and airborne data. *Journal of Glaciology*, 55(190), 245-257.

Kääb, A. & Funk, M., 1999. Modelling mass balance using photogrammetric and geophysical data: a pilot study at Griesgletscher, Swiss Alps. *The Journal of glaciology*, 45(151), 575-583.

Kennett, M. & Eiken, T., 1997. Airborne measurement of glacier surface elevation by scanning laser altimeter . *Annals of Glaciology*, 24, 293-296.

Kirk, R.L., 2003. ISIS Photoclinometry User Guide.

Kirk, R.L., Barrett, J.M. & Soderblom, L.A., 2003a. Photoclinometry made simple...? *Advances in Planetary Mapping 2003*.

Kirk, R.L., Howington-Kraus, E. et al., 2003b. High-resolution topomapping of candidate MER landing sites with MOC: New Results and Error Analyses. *Lunar and Planetary Science*, 34.

Kirkbride, M.P., 2002. Icelandic Climate and Glacier Fluctuations Through the Termination of the "Little Ice Age". *Polar Geography*, 26, 116-133.

Kirkbride, M.P. & Dugmore, A.J., 2006. Responses of mountain ice caps in central Iceland to Holocene climate change. *Quaternary Science Reviews*, 25(13-14), 1692-1707.

Kirkbride, M.P. & Dugmore, A.J., 2008. Two millennia of glacier advances from southern Iceland dated by tephrochronology. *Quaternary Research*, 70(3), 398-411.

Krabill, W. et al., 2000. Greenland Ice Sheet: High-Elevation Balance and Peripheral Thinning. *Science*, 289(5478), 428-430.

Krabill, W. et al., 2002. Aircraft laser altimetry measurement of elevation changes of the greenland ice sheet: technique and accuracy assessment. *Journal of Geodynamics*, 34(3-4), 357-376.

Krabill, W. et al., 1999. Rapid Thinning of Parts of the Southern Greenland Ice Sheet. *Science*, 283(5407), 1522-1524.

Krabill, W., Thomas, R.H., Jezek, K. et al., 1995a. Greenland ice sheet thickness changes measured by laser altimetry. *Geophysical Research Letters*, 22(17), 2341-2344.

Krabill, W., Thomas, R.H., Martin, C. et al., 1995b. Accuracy of airborne laster altimetry over the greenland ice sheet. *International Journal of Remote Sensing*, 16(7), 1211-1222.

Krimmel, R.M., 1999. Analysis of Difference between Direct and Geodetic Mass Balance Measurements at South Cascade Glacier, Washington. *Geografiska Annaler. Series A, Physical Geography*, 81(4), 653-658.

Lapen, D.R. & Martz, L.W., 1996. An investigation of the spatial association between snow depth and topography in a Prairie agricultural landscape using digital terrain analysis. *Journal of Hydrology*, 184, 277-298.

Latypov, D., 2002. Estimating relative lidar accuracy information from overlapping flight lines. *ISPRS Journal of Photogrammetry and Remote Sensing*, 56(4), 236-245.

Levin, N., Ben-Dor, E. & Karnieli, A., 2004. Topographic information of sand dunes as extracted from shading effects using Landsat images. *Remote Sensing of Environment*, 90, 190-209.

Licciardi, J.M., Kurz, M.D. & Curtice, J.M., 2007. Glacial and volcanic history of Icelandic table mountains from cosmogenic 3He exposure ages. *Quaternary Science Reviews*, 26(11-12), 1529-1546.

Liu, H., 2003. Derivation of surface topography and terrain parameters from single satellite image using shape-from-shading technique. *Computers & Geosciences*, 29(10), 1229-1239.

Liu, X., 2008. Airborne LiDAR for DEM generation: some critical issues. *Progress in Physical Geography*, 32(1), 31-49.

Lohse, V., Heipke, C. & Kirk, R.L., 2006. Derivation of planetary topography using multi-image shape-from-shading. *Planetary and Space Science*, 54(7), 661-674.

Magnússon, E. et al., 2005. The 20th century retreat of ice caps in Iceland derived from airborne SAR: W-Vatnajökull and N-Myrdalsjökull. *Earth and Planetary Science Letters*, 237(3-4), 508-515.

Magnússon, E. et al., 2004. Glaciological application of InSAR topography data of western Vatnajökull. *Jökull* , 54, 17-36.

Magnússon, E. et al., 2005. Volume changes of Vatnajökull ice cap, Iceland, due to surface mass balance, ice flow, and subglacial melting at geothermal areas. *Geophysical Research Letters*, 32, L05504.

Markham, B.L. et al., 2005. SLC-off Landsat-7 ETM+ reflective band radiometric calibration. In *Earth Observing Systems X*. San Diego, CA, USA: SPIE, pp. 58820D-11. Available at: http://link.aip.org/link/?PSI/5882/58820D/1 [Accessed February 16, 2009].

Maxwell, S.K., Schmidt, G.L. & Storey, J.C., 2007. A multi-scale segmentation approach to filling gaps in Landsat ETM+ SLC-off images. *International Journal of Remote Sensing*, 28(23), 5339-5356.

McKinzey, K.M., Ólafsdóttir, R. & Dugmore, A.J., 2005a. Perception, History, and Science: Coherence or Disparity in the Timing of the Little Ice Age Maximum in Southeast Iceland? *Polar Record*, 41(04), 319-334.

McKinzey, K.M., Orwin, J.F. & Bradwell, T., 2005b. A revised chronology of key Vatnajokull (Iceland) outlet glaciers during the Little Ice Age. *Annals of Glaciology*, 42, 171-179.

Meier, M.F. et al., 2007. Glaciers dominate eustatic sea-level rise in the 21st century. *Science*, 317, 1064-1067.

Miller, M.M. & Pelto, M.S., 1999. Mass Balance Measurements on the Lemon Creek Glacier, Juneau Icefield, Alaska 1953-1998. *Geografiska Annaler. Series A, Physical Geography*, 81(4), 671-681.

Miller, M.M. & Pelto, M.S., 1990. Mass Balance of the Taku Glacier, Alaska from 1946 to 1986. *Northwest Science*, 64(3), 121-130.

Muskett, R. et al., 2009. Airborne and spaceborne DEM- and laser altimetry-derived surface elevation and volume changes of the Bering Glacier system, Alaska, USA, and Yukon, Canada, 1972-2006. *Journal of Glaciology*, 55(190), 316-326.

Norðdahl, H. et al., 2008. Late Weichselian and Holocene environmental history of Iceland. *Jökull* , 58, 343-364.

Nuth, C. et al., 2007. Glacier geometry and elevation changes on Svalbard (1936-90): a baseline dataset. *Annals of Glaciology*, 46, 106-116.

Oerlemans, J. et al., 2005. Estimating the contribution of Arctic glaciers to sea-level change in the next 100 years. *Annals of Glaciology*, 42, 230-236.

Pacquerault, S. & Maitre, K., 1998. A new method for backscatter model estimation and elevation map computation using radarclinometry. In *Proceedings of the SPIE - The International Society for Optical Engineering*. Barcelona, Spain, pp. 230-241.

Patterson, W.S.B., 1981. *The Physics of Glaciers* 2nd ed., Oxford: Pergamon Press.

Pelto, M.S. & Riedel, J., 2001. Spatial and temporal variations in annual balance of North Cascade glaciers, Washington 1984-2000. *Hydrological Processes*, 15(18), 3461-3472.

Rasmussen, L.A., 2005. Mass balance of Vatnajökull reconstructed back to 1958. *Jökull* , 55, 139-146.

Rasmussen, L.A. & Kohler, J., 2007. Mass balance of three Svalbard glaciers reconstructed back to 1948. *Polar Research*, 26(2), 168-174.

Rasmussen, L.A. & Krimmel, R.M., 1999. Using Vertical Aerial Photography to Estimate Mass Balance at a Point. *Geografiska Annaler. Series A, Physical Geography*, 81(4), 725-733.

Raup, B., Scambos, T.A. & Haran, T.R., 2005. Topography of streaklines on an Antarctic ice shelf from photoclinometry applied to a single Advanced Land Imager (ALI) image. *Geoscience and Remote Sensing, IEEE Transactions on*, 43(4), 736-742.

Rees, W.G., 1992. Measurement of the fractal dimension of ice-sheet surfaces using Landsat data. *International Journal of Remote Sensing*, 13(4), 663-671.

Rees, W.G., 2006. *Remote Sensing of Snow and Ice*, Boca Raton: Taylor & Francis.

Rees, W.G., 2000. The accuracy of Digital Elevation Models interpolated to higher resolutions. *International Journal of Remote Sensing*, 21(1), 7.

Rees, W.G. & Arnold, N.S., 2007. Mass Balance and Dynamics of a Valley Glacier Measured by High-Resolution LiDAR. *Polar Record*, 43(04), 311-319.

Rees, W.G. & Dowdeswell, J.A., 1988. Topographic effects on light scattering from snow. *Proceedings of IGARSS '88 Symposium, Edinburgh, Scotland, 13-16 Sept.*, 161-164.

Reza, M.M. & Ali, S.N., 2008. Using IRS Products to Recover 7ETM+ Defective Images. *American Journal of Applied Sciences*, 5(6), 618-625.

Richardson, C. & Holmlund, P., 1999. Spatial variability at shallow snow-layer depths in central Dronning Maud Land, East Antarctica. *Annals of Glaciology*, 29, 10-16.

Richardson, S.D. & Reynolds, J.M., 2000. An overview of glacial hazards in the Himalayas. *Quaternary International*, 65-66, 31-47.

Rignot, E. et al., 2008. Recent Antarctic ice mass loss from radar interferometry and regional climate modelling. *Nature Geosci*, 1(2), 106-110.

Rignot, E., Echelmeyer, K. & Krabill, W., 2001. Penetration Depth of Interferometric Synthetic-Aperture Radar Signals in Snow and Ice. *Geophysical Research Letters*, 28(18), PAGES 3501–3504.

Rippin, D. et al., 2003. Changes in geometry and subglacial drainage of Midre Lovenbreen, Svalbard, determined from digital elevation models. *Earth Surface Processes and Landforms*, 28(3), 273-298.

Roy, D.P. et al., 2008. Multi-temporal MODIS-Landsat data fusion for relative radiometric normalization, gap filling, and prediction of Landsat data. *Remote Sensing of Environment*, 112(6), 3112-3130.

Sapiano, J., Harrison, W.D. & Echelmeyer, K., 1998. Elevation, volume and terminus changes of nine glaciers in North America. *Journal of Glaciology*, 44(146), 119-135.

Sauber, J. et al., 2005. Ice elevations and surface change on the Malaspina Glacier, Alaska. *Geophysical Research Abstracts*, 32, L23S01-L23S04.

Scambos, T.A. et al., 2004. Glaciological Characteristics of Institute Ice Stream Using Remote Sensing. *Antarctic Science*, 16(02), 205-213.

Scambos, T.A. & Fahnestock, M.A., 1998. Improving digital elevation models over ice sheets using AVHRR-based photoclinometry. *Journal of Glaciology*, 44(146), 97-103.

Scambos, T.A. & Haran, T.R., 2002. An image-enhanced DEM of the Greenland ice sheet J. G. Winther & R. Solberg, eds. *Annals of Glaciology*, 34, 291-298.

Scambos, T.A., Nereson, N.A. & Fahnestock, M.A., 1998. Detailed topograpy of Roosevelt Island and Siple Dome, West Antarctica. *Annals of Glaciology*, 27, 61-67.

Schneider, C., 1999. Energy balance estimates during the summer season of glaciers of the Antarctic Peninsula. *Global and Planetary Change*, 22, 117-130.

Schowengerdt, R.A., 2007. *Remote Sensing: Models and Methods for Image Processing* 3rd ed., London: Academic Press.

Shook, K. & Gray, D.M., 1996. Small-scale spatial structures of shallow snowcovers. *Hydrological Processes*, 10, 1283-1292.

Sigurðsson, O., 1998. Glacier variations in Iceland 1930-1995. *Jökull* , 45, 3-25.

Sigurðsson, O., 2000. Jöklabreytingar 1930-1960, 1960-1990, og 1997-1998. *Jökull* , 49, 83-90.

Sigurðsson, O., 2002. Jöklabreytingar 1930-1960, 1960-1990, og 1999-2000. *Jökull*, 51, 79-86.

Sigurðsson, O., 2003. Jöklabreytingar 1930-1960, 1960-1990, og 2000-2001. *Jökull* , 52, 61-67.

Sigurðsson, O., 2004. Jöklabreytingar 1930-1960, 1960-1990, og 2003-2003. *Jökull* , 54, 75-83.

Sigurðsson, O., 2005. Jöklabreytingar 1930-1960, 1960-1990, og 2003-2004. *Jökull* , 55.

Sigurðsson, O., 2006. Jöklabreytingar 1930-1970, 1970-1995, 1995-2004, og 2004-2005. *Jökull* , 56, 85-93.

Sigurðsson, O. & Jónsson, T., 1995. Relation of glacier variations to climate changes in Iceland. *Annals of Glaciology*, 21, 263-270.

Simonetto, E., Oriot, H. & Garello, R., 1999. 3D extraction from airborne SAR imagery. In *Proceedings of the SPIE - The International Society for Optical Engineering*. Florence, Italy, pp. 400-411.

Simonetto, E., Oriot, H. & Garello, R., 2000. Potentiality of high-resolution SAR images for radargrammetric applications. In *ESA Special Publications*. Toulouse, France, pp. 173-178.

Sjöberg, L.E. et al., 2004. Land uplift near Vatnajökull, Iceland, as observed by GPS in 1992, 1996 and 1999. *Geophysical Journal International*, 159(3), 943-948.

Surazakov, A. & Aizen, V., 2006. Estimating Volume Change of Mountain Glaciers Using SRTM and Map-Based Topographic Data. *Geoscience and Remote Sensing, IEEE Transactions on*, 44(10), 2991-2995.

Thomas, J., Kober, W. & Leberl, F., 1991. Multiple Image SAR Shape-from-shading. *Photogrammetric Engineering and Remote Sensing*, 57(1), 51-59.

VanLooy, J., Forster, R. & Ford, A., 2006. Accelerating thinning of Kenai Peninsula glaciers, Alaska. *Geophysical Research Letters*, 33, L21307.

Warren, S.G., 1982. Optical Properties of Snow. *Reviews of Geophysics and Space Physics*, 20(1), 67-89.

Williams, R.S. et al., 1997. Comparison of satellite-derived with ground-based measurements of the fluctations of the margins of Vatnajokull, Iceland 1973-92. *Annals of Glaciology*, 24, 72-80.

Yang, J. & Li, D., 2003. A study on the extraction of DEM from single SAR image. In *Proceedings of the SPIE - The International Society for Optical Engineering*. Beijing, China, pp. 676-679.

Wulder, M.A. et al., 2008. Evaluation of Landsat-7 SLC-off image products for forest change detection. *Canadian Journal of Remote Sensing*, 34(2), 93-99.

Zagorski, P. et al., 2008. Changes in the extent and geometry of the Scott Glacier, Spitsbergen. *Polish Polar Research*, 29(2), 163-185.

Zhang, R. et al., 1999. Shape-from-shading: a survey. *Pattern Analysis and Machine Intelligence, IEEE Transactions on*, 21(8), 690-706.

Zwally, H.J. et al., 2002. ICESat's laser measurements of polar ice, atmosphere, ocean, and land. *Journal of Geodynamics*, 34(3-4), 405-445.

Zwally, H.J. et al., 1983. Surface Elevation Contours of Greenland and Antarctic Ice Sheets. *Journal of Geophysical Research*, 88(C3), 1589-1596.

Zwally, H.J. et al., 2005. Mass changes of the Greenland and Antarctic ice sheets and shelves and contributions to sea-level rise: 19922002. *Journal of Glaciology*, 51, 509-527.